

Final Report: Evaluation and Geologic Validation of EO-1 Hyperion (NASA Grant NCC5-495)

**F. A. Kruse and J. W. Boardman¹
And
J. F. Huntington²**

Submitted 03/14/2003

¹ Analytical Imaging and Geophysics LLC (AIG), 4450 Arapahoe Ave, Suite 100, Boulder, Colorado 80303, (e-mail: kruse@aigllc.com)

² Commonwealth Scientific & Industrial Research Organisation (CSIRO), Division of Exploration and Mining, North Ryde, NSW, Australia, 2113

Table of Contents

EXECUTIVE SUMMARY.....	3
1.0 OBJECTIVES.....	4
2.0 BACKGROUND – THE HYPERSPECTRAL MINERAL MAPPING PROCESS....	5
3.0 GEOLOGIC VALIDATION SUMMARIES.....	10
Los Menucos, Argentina.....	13
Cuprite, NV.....	20
Virginia City, NV.....	26
Steamboat Springs, NV.....	29
Oatman, AZ.....	34
Northern Death Valley, CA/NV.....	40
4.0 SUMMARY OF KEY RESEARCH RESULTS.....	46
5.0 RESEARCH SIGNIFICANCE.....	47
6.0 KRUSE ET-AL EO-1 HYPERION PUBLICATIONS.....	48
7.0 ACKNOWLEDGEMENTS.....	49
8.0 REFERENCES CITED.....	49

EXECUTIVE SUMMARY

AIG, in cooperation with CSIRO, Sydney Australia has evaluated, validated, and demonstrated Hyperion hyperspectral data for geologic applications. Three test sites were originally proposed for analysis, the northern Grapevine Mountains, Nevada (northern Death Valley CA/NV); Oatman, Arizona; and Virginia City, Nevada. Hyperion data analysis was conducted for these sites along with additional sites added to the study based on data availability. The additional sites are the Los Menucos area, Argentina; Steamboat, NV; and Cuprite, Nevada. Cumulatively, these test sites provide geologically diverse terrains allowing validation of Hyperion data across a variety of geologic environments. Airborne Visible/Infrared Imaging Spectrometer (AVIRIS) data served as the baseline for comparative determination of Hyperion data characteristics and performance. Previous field and airborne mapping and spectral characterization allowed AIG/CSIRO to assess Hyperion suitability and performance for geologic mapping and mineral resource appraisal. Results over sites with established ground truth and years of airborne hyperspectral data show that Hyperion data from the short-wave-infrared (SWIR) spectrometer can be used to produce useful geologic (mineralogical) information. Minerals mapped include carbonates, chlorite, epidote, kaolinite, alunite, buddingtonite, muscovite, hydrothermal silica, and zeolite. Data collected under optimum conditions (summer season, bright targets, well-exposed geology) indicate that Hyperion meets pre-launch specifications and allows subtle distinctions such as determining the difference between calcite and dolomite and mapping solid solution differences in micas caused by substitution in octahedral molecular sites. Comparison of airborne hyperspectral data (AVIRIS) to the Hyperion data establishes that Hyperion provides similar basic mineralogical information, with the principal limitation being reduced mapping of fine spectral detail under less-than-optimum acquisition conditions (winter season, dark targets) based on lower signal-to-noise ratios (SNR). The case histories demonstrate the analysis methodologies and level of information available from the Hyperion data. They also show the viability of Hyperion as a means of extending hyperspectral mineral mapping to areas not accessible to aircraft sensors. The analysis results demonstrate that spaceborne hyperspectral sensors can produce useful mineralogical information, but also indicate that SNR improvements are required of future spaceborne sensors to allow the same level of mapping that is currently possible from airborne sensors such as AVIRIS. Results from this research provide valuable information about hyperspectral sensing from space that can be used to help bootstrap future hyperspectral satellite missions.

1.0 OBJECTIVES

Original Objectives from the Proposal

AIG/CSIRO's original objectives for the Hyperion research were:

1. To evaluate Hyperion to determine its performance and to validate with respect to requirements for applied and commercial use of space-based hyperspectral data. Specifically, we proposed to evaluate, validate, and demonstrate Hyperion in the role of geologic mapping and in the context of monitoring the processes that control the occurrence of non-renewable mineral resources.
2. To examine the issues of spectral and spatial scaling using Hyperion data. We proposed to use Hyperion data to examine scaling issues inherent to analysis of satellite hyperspectral data (subpixel detection, identification, quantification, and mapping) and to validate Hyperion through comparison with airborne hyperspectral datasets, laboratory and field spectral measurements, and ARIES-1 simulations.

The AIG/CSIRO proposal was for evaluation, validation, and demonstration of Hyperion's capabilities for geologic mapping and mineral resource assessment, offering a low-cost, high-experience, high-leverage approach. The effort drew heavily on previous work and outside funding sources to maximize the cost-effectiveness for the Hyperion evaluation and validation. Key results were achieved by examining Hyperion data collected over well-understood geological sites. Results include 1) practical and important demonstrations of Hyperion data for geological mapping and mineral resource assessment; 2) validation of the spatial, spectral and radiometric performance of Hyperion using real-world applications as the defining metric; 3) validation of analysis methods originally developed for airborne hyperspectral data for use with satellite-based sensors.

The following restatement of the project objectives provides a simplified overview of the driving factors behind the analysis:

Restated Objectives

1. To evaluate Hyperion's capacity to map known geology and alteration mineralogy exposed at various geologic validation sites
2. To compare this capacity against other hyperspectral data / systems and ground truth
3. With the aim of understanding Hyperion performance and matching future sensor needs against geologic applications and requirements

2.0 Background: The Hyperspectral Mineral Mapping Process

The methods described here illustrates AIG's approach to mineral mapping using hyperspectral data. These methods have been tested extensively using AVIRIS and other airborne hyperspectral datasets. The Hyperion data analysis represents the first time that this approach has been applied to satellite hyperspectral datasets.

We believe that hyperspectral data analysis should be cast in the same format as other geophysical data analysis processes. First, the data must be fully calibrated and well characterized. Then instrumental and natural influences on the data, unrelated to our signal of interest, should be modeled and removed via a data reduction step. We use a spectral mixing model to derive the locations and spectral signatures of various key scene components. These derived components, or endmembers, are identified using spectral matching methods and their apparent abundances mapped over the entire hyperspectral scene. Finally, the results are geometrically rectified and map registered. These steps are shown schematically in Figure 1. The details of the methodology are described in the following sections.

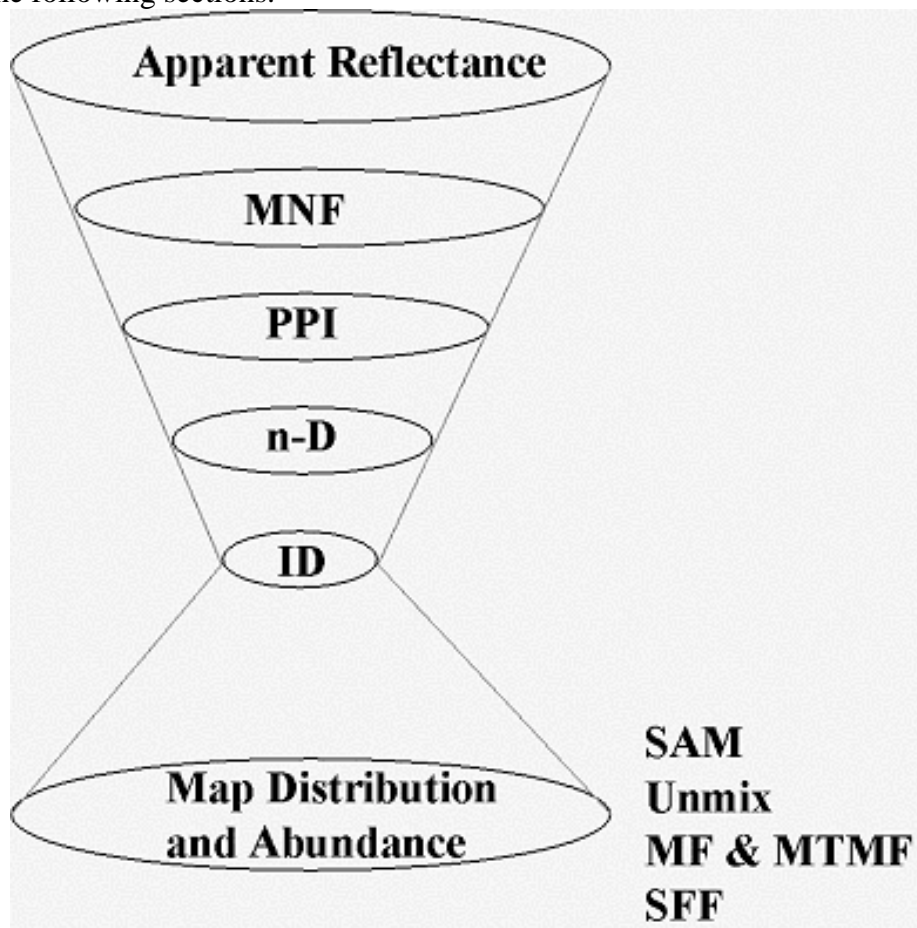


Figure 1: AIG Hyperspectral Analysis Scheme. Note the "hourglass" shape, which schematically represents the reduction of the hyperspectral data to just a few key spectra at the "neck" and then expansion back to spectral maps of the full dataset.

Analytical Imaging and Geophysics LLC (AIG) has evolved a “standardized” hyperspectral data analysis methodology (Figure 1) that has been tested for a variety of data (Boardman et al., 1995; Kruse et al., 1996a,b; Kruse et al., 2001). These approaches are implemented and documented within the “Environment for Visualizing Images” (ENVI) software system originally developed by AIG scientists (now an Eastman Kodak/Research Systems Inc [RSI] commercial-off-the-shelf [COTS] product) (Research Systems Inc, 2001). They are also briefly described below. This is not the only way to analyze these data, but we have found that it provides a consistent way to extract spectral information from hyperspectral data without a priori knowledge or requiring ground observations. The analysis approach consists of the following steps:

1. correction for atmospheric effects using an atmospheric model “ACORN” (AIG, 2001)
2. spectral compression, noise suppression, and dimensionality reduction using the Minimum Noise Fraction (MNF) transformation (Green et al., 1988; Boardman, 1993),
3. determination of potential endmembers (unique spectra) using geometric methods (Pixel Purity Index – “PPI”) (Boardman and Kruse, 1994; Boardman et al., 1995)
4. extraction of endmember spectra using n-dimensional scatter plotting (Boardman et al., 1995)
5. identification of endmember spectra using visual inspection, automated identification, and spectral library comparisons (Clark et al., 1990; Kruse and Lefkoff, 1993; Kruse et al., 1993a)
6. production of mineral maps using a variety of mapping methods - the “Spectral Angle Mapper” (SAM) (Kruse et al., 1993b) and “Mixture-Tuned-Matched-Filtering” (MTMF) (Boardman, 1998) were used for this study. The final step also usually included geocorrection of the data to map coordinates.

Atmospheric Corrections are a Prerequisite for Most Analysis

Remote sensing measurements of the Earth's surface are strongly influenced by the atmosphere (Goetz et al., 1985). Both scattering and absorption by gases and particulates affect the amount and wavelengths of light reaching the sensors. Absorption by atmospheric gases is dominated by water vapor with smaller contributions from carbon dioxide, ozone, and other gases (Gao and Goetz, 1990). Strong atmospheric water absorption bands make the atmosphere opaque in many regions (for example the 1.4 and 1.9 μm regions) and only small atmospheric windows are available for terrestrial remote sensing.

One of the most critical steps in most imaging spectrometer data analysis strategies is to convert the data to reflectance, principally so that individual spectra can be compared directly with laboratory or field data for identification. Our analysis methods are generally applicable to both airborne and satellite data, however, the methodology requires processing radiance-calibrated data to apparent reflectance. (If comparison to reflectance isn't required, then this step may be eliminated, but for most work, this is a requirement). Ideally, imaging spectrometer data should be calibrated to absolute reflectance using onboard calibration. Onboard calibration, however, is typically not available.

Atmospheric CORrection Now (ACORN), currently used for correction of both airborne and satellite hyperspectral data, is a commercially-available, enhanced atmospheric model-based software that uses licensed MODTRAN4 technology to produce high quality surface reflectance without ground measurements (AIG, 2001). The AVIRIS and Hyperion data used in our analyses were both converted to apparent reflectance using ACORN. Appropriate model parameters for each instrument (eg: sensor altitude), collection date (eg: date, time, seasonal atmospheric model), and location (eg: latitude/longitude, average elevation) were used, otherwise, all other parameters were identical for both datasets. The output of ACORN is an image showing the spatial distribution of

various water vapor concentrations as derived for each pixel of the AVIRIS data and scaled surface apparent reflectance. This method makes it possible to quantitatively derive physical parameters and analyze data from different regions and different times without *a priori* knowledge. We can also compare and analyze imaging spectrometry data acquired by different instruments, compare to field and laboratory spectral measurements, or to spectra generated using theoretical models. Correction to reflectance was critical for analysis of the Hyperion data.

MNF Transform

A “Minimum Noise Fraction” (MNF) Transform is used to reduce the number of spectral dimensions to be analyzed. The MNF transformation is a linear transformation related to principal components that orders the data according to signal-to-noise-ratio (Green et al., 1988). It can be used to determine the inherent dimensionality of the data, to segregate noise in the data, and to reduce the computational requirements for subsequent processing (Green et al., 1988; Boardman and Kruse, 1994). The MNF transformation can be used to partition the data space into two parts: one associated with large eigenvalues and coherent eigenimages, and a second with near-unity eigenvalues and noise-dominated images. By using only the coherent portions in subsequent processing, the noise is separated from the data, thus improving spectral processing results.

Pixel Purity Index (PPI)

Based on MNF results, the lower order MNF bands are usually set aside and the higher order bands selected for further processing. These are used in the “Pixel Purity Index” (PPI), processing designed to locate the most spectrally extreme (unique or different or “pure”) pixels (Boardman et al., 1995). The most spectrally pure pixels typically correspond to mixing endmembers. The PPI is computed by repeatedly projecting n-dimensional scatterplots onto a random unit vector. The extreme pixels in each projection are recorded and the total number of times each pixel is marked as extreme is noted. A PPI image is created in which the digital number of each pixel corresponds to the number of times that pixel was recorded as extreme. A histogram of these images shows the distribution of “hits” by the PPI. A threshold is interactively selected using the histogram and used to select only the purest pixels in order to keep the number of pixels to be analyzed to a minimum. These pixels are used as input to an interactive visualization procedure for separation of specific endmembers.

n-Dimensional Visualization

Spectra can be thought of as points in an n-dimensional scatterplot, where n is the number of bands (Boardman, 1993; Boardman et al., 1995). The coordinates of the points in n-space consist of “n” values that are simply the spectral reflectance values in each band for a given pixel. The distribution of these points in n-space can be used to estimate the number of spectral endmembers and their pure spectral signatures, and provides an intuitive means to understand the spectral characteristics of materials. In two dimensions, if only two endmembers mix, then the mixed pixels will fall in a line in the histogram. The pure endmembers will fall at the two ends of the mixing line. If three endmembers mix, then the mixed pixels will fall inside a triangle, four inside a tetrahedron, and so on. Mixtures of endmembers “fill in” between the endmembers. All mixed spectra are “interior” to the pure endmembers, inside the simplex formed by the endmember vertices, because all the abundances are positive and sum to unity. This “convex set” of mixed pixels can be used to determine how many endmembers are present and to estimate their spectra.

In practice, the thresholded pixels from the MNF images are loaded into an n-dimensional scatterplot and rotated in real time on the computer screen until “points” or extremities on the scatterplot are exposed. These projections are “painted” using Region-of-Interest (ROI) definition procedures and then rotated again in 3 or more dimensions (3 or more bands) to determine if their signatures are unique in the MNF data. Once a set of unique pixels are defined, then each separate projection on

the scatterplot (corresponding to a pure endmember) is exported to a ROI in the image. Mean spectra are then extracted for each ROI to act as endmembers for spectral mapping.

Spectral Identification

Spectral identification of the endmembers extracted using the n-dimensional scatterplotting is based on a combination of visual inspection of spectral plots and manual/automated comparison to spectral libraries (Clark et al., 1990, Kruse and Lefkoff, 1993, Kruse et al., 1993a). Spectra are visually examined to identify key spectral features locations, depths, and shapes, and these are compared against application-specific spectral libraries. Automated methods that compare overall spectral shape and specific features are also applied to determine candidate materials and to produce mathematical comparisons. Once names have been assigned to individual endmember spectra, then these can be passed forward to the spectral/spatial mapping algorithms.

Mapping Methods

AIG uses a variety of mapping methods depending on the data type and the desired results. The Spectral Angle Mapper (SAM) Classification and Mixture-Tuned Matched Filtering were used for this research. The Spectral Angle Mapper (SAM) is an automated method for comparing image spectra to individual spectra (Boardman, Unpublished data; Kruse et al., 1993b). The algorithm determines the similarity between two spectra by calculating the spectral angle between them, treating them as vectors in a space with dimensionality equal to the number of bands. Because this method uses only the vector direction of the spectra and not their vector length, the method is insensitive to illumination. The result of the SAM classification is a color-coded image showing the best SAM match (the predominant material) at each pixel. Additionally, rule images are calculated that show the actual angular distance (in radians) between each spectrum in the image and each reference or endmember spectrum in n-dimensional space. Darker pixels in the rule images represent smaller spectral angles and thus spectra that are more similar to the endmember spectra. For the purposes of display, the dark pixels are inverted, so that the best matches appear bright. These images present a good first cut of the spatial distribution of spectrally unique materials.

Geologic surfaces are rarely composed of a single uniform material, however, thus it may be necessary to use mixture modeling to determine what materials cause a particular spectral “signature” in imaging spectrometer data. Spectral mixing is a consequence of the mixing of materials having different spectral properties within a single image pixel. If the scale of the mixing is large (macroscopic), then the mixing occurs in a linear fashion. A simple additive linear model can be used to estimate the abundances of the materials measured by the imaging spectrometer. Each mixed spectrum is a linear combination of the "pure" spectra, each weighted by their fractional abundance within the pixel, a simple averaging (Boardman, 1989).

While the SAM algorithm does provide a means of identifying and spatially mapping materials, it only picks the best match to a given spectrum. Mixture-Tuned Matched Filtering is a hybrid method based on the combination of well-known signal processing methodologies and linear mixture theory. Matched filtering (MF), based on well-known signal processing methodologies, maximizes the response of a known endmember and suppresses the response of the composite unknown background (Harsanyi and Chang, 1994). MF also provides a rapid means of detecting specific minerals based on matches to specific library or image endmember spectra, again, however, it fails to consider spectral mixing. Matched filter results are usually presented as gray-scale images with values from 0 to 1.0, which provide a means of estimating relative degree of match to the reference spectrum (where 1.0 is a perfect match). Earth surfaces, however, are rarely composed of a single uniform material, thus it is usually necessary to consider mixture modeling to determine what materials cause a particular spectral “signature” in imaging spectrometer data (Boardman et al., 1995). Mixture-Tuned-Matched-Filtering (MTMF) utilizes the MF theory above, but also includes a simple additive linear mixing model to estimate the abundances of the materials measured by the

hyperspectral sensor (Boardman, 1998) – in effect performing partial unmixing. Two dimensional scatterplotting of the MF score versus the MTMF Infeasibility score can be used to produce color-coded maps for materials occurring above specific abundance thresholds. Individual grayscale MF images can be used to show material abundances.

The AIG methods described above demonstrate how the inherent information in imaging spectrometry data can be extracted. It should be noted, however, that if the spectral signatures to be mapped are already known, and hyperspectral data and endmember spectra are properly scaled, then AIG's advanced mapping methods can be applied directly without going through the entire data-reduction procedure. Additionally, we would like to reiterate that this is not the only way to analyze these data, but we have found that it provides a consistent way to extract spectral information from hyperspectral data without a priori knowledge or requiring ground observations.

3.0 GEOLOGIC VALIDATION SUMMARIES

The Airborne Visible/Infrared Imaging Spectrometer (AVIRIS) represents the current state of the art airborne hyperspectral system and our principal “ground truth” (along with selected ground spectral measurements) for this investigation. AVIRIS, flown by NASA/Jet Propulsion Laboratory (JPL) is a 224-channel imaging spectrometer with approximately 10 nm spectral resolution covering the 0.4 – 2.5 μm spectral range (Green et al., 1999). The sensor is a whiskbroom system utilizing scanning foreoptics to acquire cross-track data. The IFOV is 1 milliradian. Four off-axis double-pass Schmidt spectrometers receive incoming illumination from the foreoptics using optical fibers. Four linear arrays, one for each spectrometer, provide high sensitivity in the 0.4 to 0.7 μm , 0.7 to 1.2 μm , 1.2 to 1.8 μm , and 1.8 to 2.5 μm regions respectively. AVIRIS is flown as a research instrument on the NASA ER-2 aircraft at an altitude of approximately 20 km, resulting in approximately 20-m pixels and a 10.5-km swath width. Since 1998, it has also been flown on a Twin Otter aircraft at low altitude, yielding 2 – 4m spatial resolution.

For comparison, Hyperion is a satellite hyperspectral sensor covering the 0.4 to 2.5 μm spectral range with 242 spectral bands at approximately 10nm spectral resolution and 30m spatial resolution from a 705km orbit (Pearlman et al., 1999). Hyperion is a pushbroom instrument, capturing 256 spectra each with 242 spectral bands over a 7.5Km-wide swath perpendicular to the satellite motion. The system has two grating spectrometers; one visible/near infrared (VNIR) spectrometer (approximately 0.4 – 1.0 μm) and one short-wave infrared (SWIR)) spectrometer (approximately 0.9 – 2.5 μm). Data are calibrated to radiance using both pre-mission and on-orbit measurements. Key AVIRIS and Hyperion characteristics are compared in Table 1 and discussed further in Green et al., 2003.

Table 1: AVIRIS/Hyperion Sensor Characteristics Comparison

HSI Sensor	Spectral Resolution	Spatial Resolution	Swath Width	SWIR SNR
AVIRIS	10 nm	2 - 20 m	1 - 12 km	~500:1
Hyperion	10 nm	30 m	7.5 km	~50:1

Data Acquisition

Hyperion hyperspectral data were originally requested for the three primary test sites, Virginia City, NV; Oatman, AZ; and northern Death Valley, CA. Additional Hyperion validation sites were added, however, because the late November 2000 launch occurred during the northern hemisphere winter. The following is a list of Hyperion data collected and delivered in support of this investigation.

Table 2: Kruse et al. Hyperion Data collects

Los Menucos, Argentina

25 Feb 2001: EO12300882001056111PP (some clouds)
 30 Apr 2001: EO12300882001120111PP (mostly clouds)
 16 May 2001: EO12300882001136111PP (all clouds)
 1 June 2001: EO12300882001152111PP (partly clouds)
 17 June 2001: E012300882001168111PP (clear)
 3 July 2001: EO12300882001184111PP (mostly clouds)
 19 July 2001: EO12300882001200112PP (all clouds)
 10 Dec 2001: EO12300882001344111PP (mostly clouds)

New Zealand Hot Springs & Mt Tarawera

21 Dec 2000: EO10720872000355111P0 (all clouds)
21 Jan 2001: EO10720872001021111P0 (all clouds)
22 Feb 2001: EO10720872001053111P0 (all clouds)
11 Apr 2001: EO10720872001101111PP (all clouds)
29 May 2001: EO10720872001149111P0 (all clouds)
10 Mar 2001: EO10720872001069111PP (some clouds)
6 Nov 2001: EO10720872001309111P0 (mostly clouds)
21 Nov 2001: EO10720872001325111P0 (all clouds)
23 Dec 2001: EO10720872001357111PP (mostly clouds)
24 Jan 2002: EO10720872002024111P0 (clear)

Cuprite, NV

1 Mar 2001: EO10410342001060111PP (clear)

Steamboat Springs, NV

31 Mar 2001: EO10430332001090111P4 (some snow)
16 Apr 2001: EO10430332001106111P4 (all clouds)
22 Aug 2001: EO10430332001234110P4 (clear)

Northern Death Valley, NV

23 July 2001: EO10410342001204111P1 (clear)
9 Sept 2001: EO10410342001252111P1 (clear)
14 Dec 2001: EO10410342001348111P1 (cloudy)
31 Jan 2002: EO10410342002031111P1 (snow)

Virginia City, NV

2 May 2001: EO10430332001122111P3 (clear)
9 June 2001: EO10430332001170111P3 (clear)
6 Aug 2001: EO10430332001218111P3 (p. cloudy)
7 Sept 2001: EO10430332001250111P3 (clear)

Oatman, AZ

6 May 2001: EO10390362001126111P0 (clear)

SNR Calculations

The quality of digital remote sensing data is directly related to the level of system noise relative to signal strength. This is usually expressed as Signal-to-Noise Ratio (SNR), a dimensionless number that describes overall system radiometric performance (Collwell, 1983). System noise is tied to sensor design and takes into account factors such as detector performance/sensitivity, spatial/spectral resolution, and noise characteristics of the system electronics. Though the noise levels for a given sensor are generally fixed, for remote sensing data acquisition, the signal portion of the SNR is affected by other external factors such as solar zenith angle, atmospheric attenuation and scattering, and surface reflectance, which modify the signal available to the sensor (Collwell, 1983).

One common means for determining an approximate SNR for remote sensing data is to use a Mean/Standard Deviation method (Green et al., 1999, 2003). This approach requires definition of a spectrally homogeneous area, calculation of the average spectrum for that area, and determination of the spectrally distributed standard deviation for the average spectrum. SNR are normalized to 50% reflectance for comparison. SNR calculated using this method are representative of those that can be extracted directly from the data, however, SNR for bright targets may be underestimated because of

homogeneity issues at higher SNR (increasing SNR may result in breakdown of apparently homogeneous areas into multiple materials and new homogeneous areas must be selected). Slightly higher SNR values could probably be obtained through direct analysis of the data dark current signal (Green et al., 1999), an “Instrument SNR”, however, this isn’t always possible. SNR calculated using the Mean/Standard Deviation method, an “Environmental SNR” are sensitive to acquisition conditions as mentioned above, and thus should be considered lower limits on performance.

Analysis of approximately 14 Hyperion scenes from around the world using the Mean/Standard Deviation SNR method shows that there is a strong relationship between the acquisition time of year (which controls the solar zenith angle) and the SNR of the Hyperion data (Kruse et al., 2001, 2003). Calculated SNR for Hyperion SWIR data are higher in the summer and lowest in the winter (Figure 2). This has a direct effect on spectral mineral mapping, with lower SWIR SNR resulting in extraction of less detail (Kruse et al., 2001, 2002a,d, 2003). While Hyperion data with approximately 25:1 SNR (Cuprite, NV) allow basic mineral identification (no separation of within-species variability) more detail (additional endmembers) are detected and mapped using the higher SNR AVIRIS and Hyperion data (60:1 SNR) at the northern Death Valley site. This is also important for geologic/mineral mapping, because higher SNR allows separation of similar endmembers such as calcite from dolomite and within-species variability such as kaolinite vs dickite. In the northern Death Valley case, the relatively high Hyperion SNR allows detection of 3 different mica endmembers with different aluminum substitution (Kruse et al., 1999). Previous investigations have indicated that SNR is critical for this determination (Kruse, 1988; Kruse et al., 2002d).

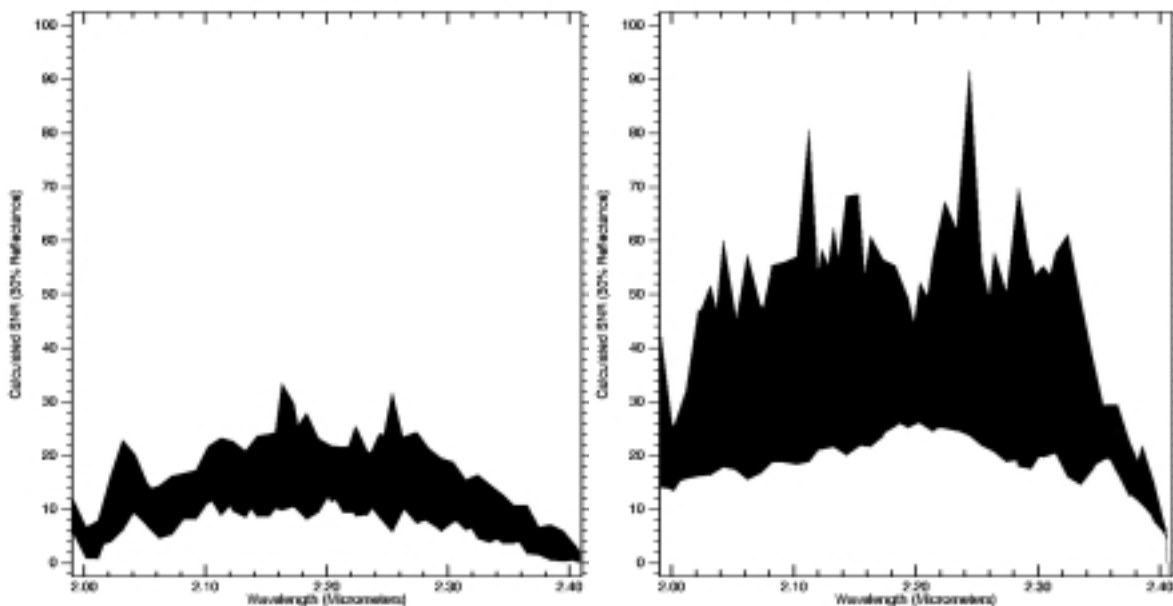


Figure 2: Comparison of Hyperion calculated SNR for “winter” data (left) and “summer” data (right). Filled areas indicate range of SNR for 14 Hyperion scenes.

Study Area Results: Los Menucos, Argentina

The Los Menucos, Rio Negro, Argentina, site (Figure 3) is a fossil analog of hot springs similar to modern systems being studied by AIG in other locations around the world. The Los Menucos gold district was discovered in 1998 by Arminex, S.A. using regional exploration methods employing Landsat Thematic Mapper (TM) satellite imagery and field investigation (Franco et al., 2000; Gemuts and Perry, 2000; Perry and Gemuts, 2000). This district has the largest significant concentration of advanced argillic, altered Permian ignimbrite and rhyolite assemblages in Argentina. Alteration is related to the intrusion of Triassic-age (?) rhyolite dome complexes below thick Permian-age felsic volcanic rocks. Associated with dome fields are large areas of phreatic breccias and hematite-rich altered oxidized zones. Alteration is characterized by vuggy silica, quartz stockwork, kaolin, and alunite. The region has potential for low-sulfidation style gold mineralization. The Los Menucos region was submitted and selected as a NASA EO-1 collection site during 2000 to evaluate other earth observation sensors, including hyperspectral (airborne AVIRIS and satellite EO-1 Hyperion) as well as multispectral data sets (Landsat 7 Enhanced Thematic Mapper and ASTER imagery). The results of the TM reconnaissance and AVIRIS analysis are presented in Kruse et al., 2002b, 2002d. The Hyperion, ETM and ASTER results are presented in Kruse et al., 2002c, 2002d.



Figure 3: Los Menucos, Argentina Site Location in Rio Negro province, Argentina. Orange box marks extent of AVIRIS survey conducted during February 2001.

AVIRIS was flown for the Los Menucos site, Argentina on a Twin Otter aircraft at low altitude on 14-15 February 2001. The AVIRIS dataset consists of 6 overlapping, approximately 2.7km x 30km north-south flightlines, at 3.5m spatial resolution. Each flightline was processed and analyzed separately in reconnaissance mode (optimized for the entire dataset, not individual sites). Two spectral ranges were analyzed; 1) 0.4–1.3 μm (iron oxides), and 2) 2.0–2.5 μm (clays, carbonates, etc). Processing consisted of standardized hyperspectral analysis as described above to allow identification and mapping of key alteration minerals. The results were map-corrected and combined into an image mosaic covering an approximately 10km x 30km area covering several key mineral prospects (Figure 4). While the complete dataset was analyzed, only several small subsections of interest are presented here: 1) Cuya, 2) and Kaolinite Hills. Other sites investigated in detail but not shown include 3) Carmen, 4) Lagunitas North, 5) Tanke Negro.

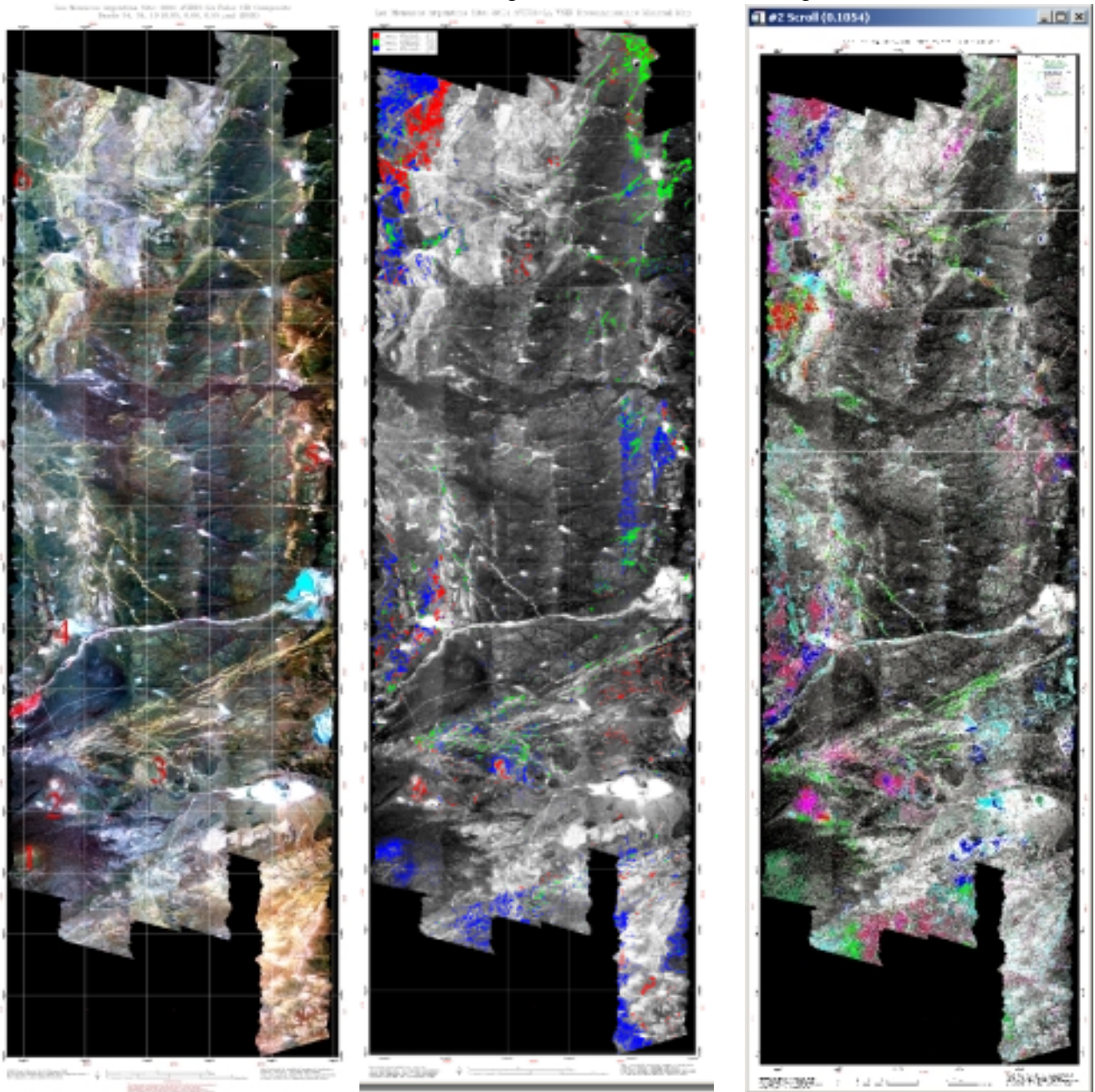


Figure 4: Left - False Color Infrared Composite (CIR) using AVIRIS bands 54, 34, 19 (0.85, 0.66, 0.55 μm) as RGB. Approximate site locations described in the text above are marked by number. Image is approximately 10 x 30kms. Center - 0.4 - 1.2 μm mineral map. Right - 2.0 - 2.5 μm mineral map.

Los Menucos Field Reconnaissance—Mineral maps (see Figure 4 and detailed images below) were used along with Landsat TM mapping as base maps for field verification. Reconnaissance was conducted during April 25 – 28, 2001 with the assistance of RTZ mining company geologists. Several prospects and other mineralogically interesting areas were visited, the rocks and alteration were examined, and samples were collected. These samples were analyzed utilizing an Analytical Spectral Devices (ASD) “FieldSpec Full Range” field spectrometer (see <http://www.asdi.com>) provided by Jet Propulsion Laboratory. The ASD spectrometer covers the 0.35 – 2.5 μm range with approximately 3nm (VNIR) and 10nm (SWIR) spectral resolution and 1nm spectral sampling. A “wand” attachment containing a halogen light source was used to illuminate the samples. This results in a high-quality spectrum with 2151 spectral bands, allowing identification of specific minerals. Over 160 spectral measurements were made of various rocks and soils from the Los Menucos area. Known mineralized areas were accurately characterized and several new prospects identified (Kruse et al., 2002d). Spectral libraries were later used to refine AVIRIS results and to apply to EO-1 Hyperion and Landsat/ASTER multispectral evaluation.

1: Cuya Prospect AVIRIS Specifics—A false color infrared (CIR) composite reference image and selected mineral maps overlain on AVIRIS band 34 (0.66 μm) were subsetted from the full AVIRIS analysis for the “Cuya” prospect (Figure 5, left). According to the AVIRIS mapping, the mineralogy at Cuya is relatively simple – mostly hydrothermal silica (massive silica) and goethite with minor muscovite (sericite). There is also evidence of minor kaolinite, montmorillonite, and calcite on disturbed surfaces based on field spectrometry (see above). The spectral plot (Figure 5, right) shows a comparison of the Cuya AVIRIS spectrum for the silica (+sericite) compared to a library spectrum of “opal” from the USGS spectral library (the closest library match). Results shown in Figures 5 and 6 are consistent with fossilized alkaline hot-springs systems. In general, the remote AVIRIS measurements agree with the ASD spectral results. Some small differences are seen in the spectra, principally caused by scaling differences (a small ASD spot of several centimeters vs the large AVIRIS pixel size of approximately 3.5m) and spectral mixing.

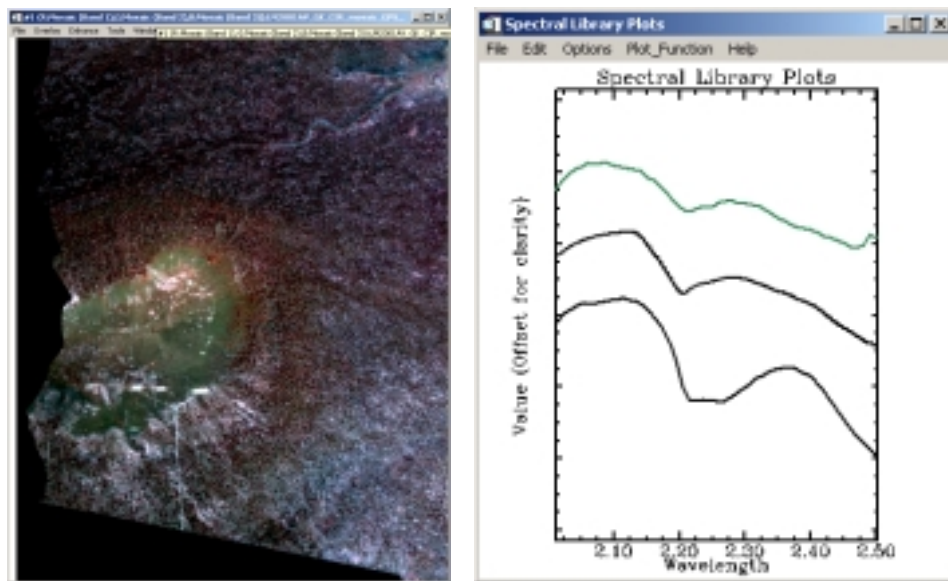


Figure 5: Cuya prospect. Left, False Color Infrared (CIR) composite image. Right, Comparison of Cuya AVIRIS spectrum (top), to ASD Field Spectrum (Middle), to USGS Library spectrum of “Opal” (bottom).

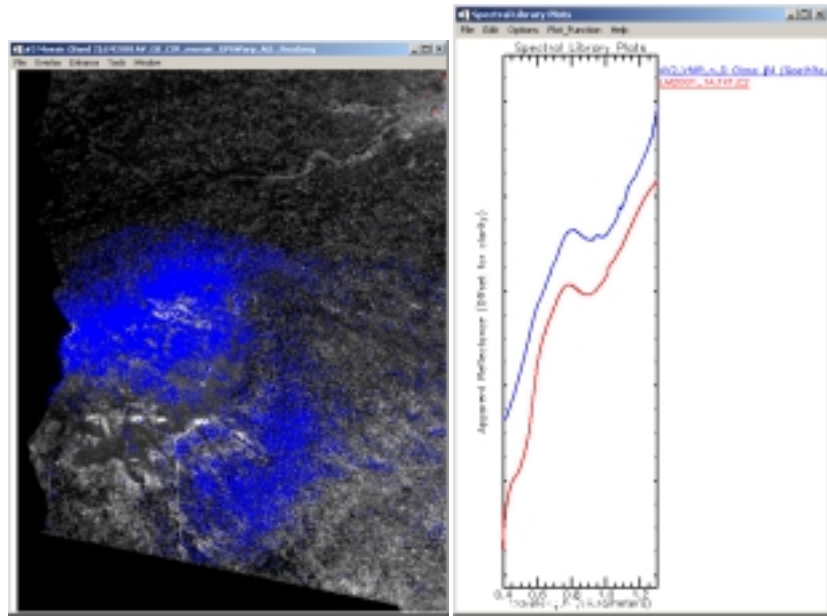


Figure 6: Cuya prospect VNIR AVIRIS mineral map and spectra. Left, VNIR Mineral map (blue=goethite). Right, comparison of AVIRIS spectrum (blue) and ASD field spectrum (red).

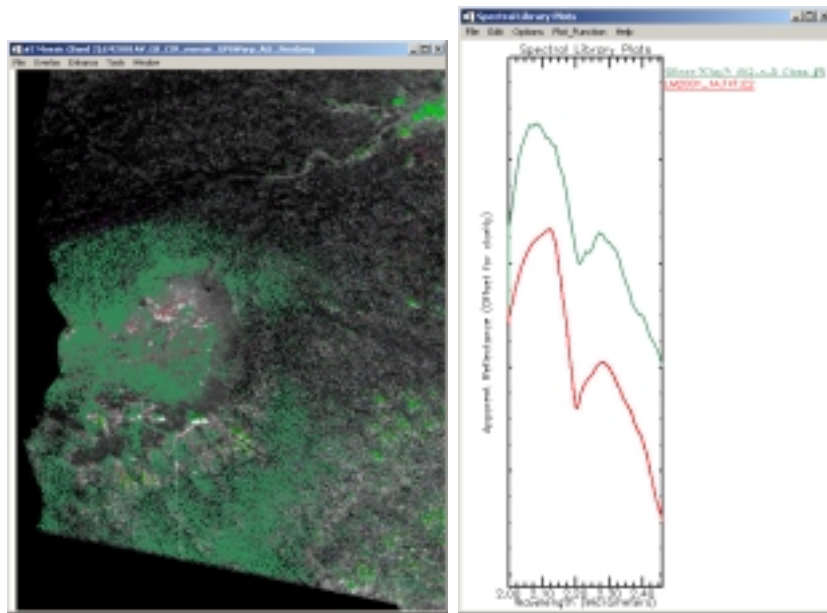


Figure 7: Cuya prospect SWIR AVIRIS mineral map and spectra. Left, SWIR mineral map (sea green=silica+-sericite). Right, comparison of AVIRIS spectrum (green) and ASD field spectrum (red).

2. Kaolinite Hills Prospect AVIRIS Specifics—AVIRIS mineral mapping identifies this as a predominantly kaolinitic area (Figure 8, 9). Mineralogy is zoned, with hematite/muscovite (sericite) in a central low area (though exposed only between up to 50%+ vegetation), surrounded by predominately well crystalline kaolinite on flanking low hills. The AVIRIS muscovite/sericite spectrum is shifted to short wavelengths (2.19 μ m) indicating probable hydrothermal origin. The ASD kaolinite spectrum matches the library kaolinite spectrum very well, though the AVIRIS spectrum is somewhat subdued, probably because of spectral mixing (Figure 8). Calcite outcrops occur both north and south of the main kaolinite areas. Several small hematite/sericite outcrops with significant silicification occur along the road just south of the principal calcite outcrops.

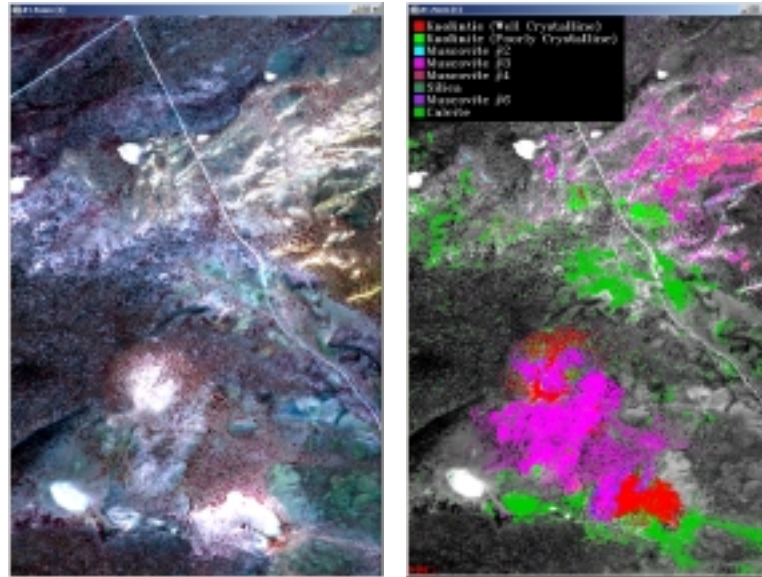


Figure 8: Kaolinite Hills prospect: Left, False Color Infrared (CIR) composite image. Right, SWIR AVIRIS mineral map. (red=kaolinite#1, bright green=kaolinite#2 [poorly crystalline], magenta=muscovite #1 [2.19 μ m], cyan=muscovite #2, Maroon=muscovite #1, sea green=silica, dark green=calcite)

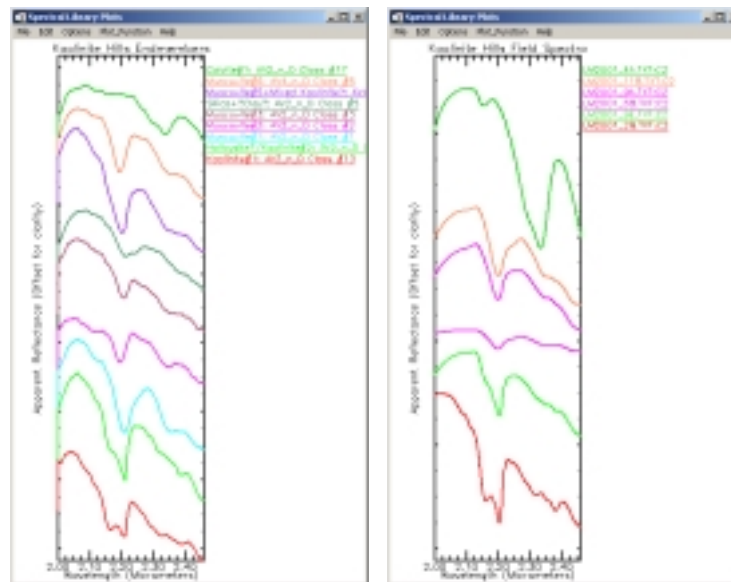


Figure 9: Comparison of AVIRIS endmember spectra (left), to ASD Field Spectrum (right). Colors are the same as Figure 8.

The high spatial resolution (3.5m) AVIRIS data allowed identification and mapping of common alteration minerals such as hematite, goethite, kaolinite, dickite, alunite, pyrophyllite, muscovite/sericite, montmorillonite, and calcite. Distinguishing between similar minerals such as kaolinite and dickite was possible because of the high SNR of the AVIRIS sensor. The AVIRIS data pointed out minerals and mineral assemblages that would not have been readily apparent utilizing conventional field mapping methods

Los Menucos, Argentina Hyperion—Hyperion data for the Los Menucos, Argentina, site were first acquired on 25 February 2001, close to the 14-15 February AVIRIS acquisition date. Unfortunately, the Hyperion data were predominantly cloudy. Additionally, Signal-to-Noise Ratios (SNR) calculated for this scene were in the 20:1 range, marginal for successful mineral identification and mapping (Kruse, 1988).

Several RTZ prospects were mostly clear on the 25 February date. These data were processed to geologic products using the AIG-developed approaches for extraction of mineralogic and geologic information. Several characteristic mineral spectra (silica, kaolinite, muscovite) were extracted from the Los Menucos Hyperion data (Figure 10). Mineral maps were produced and compared to those derived from the AVIRIS data above (Figure 10). Characteristic mineral spectra were extracted from the 25 February Hyperion data for silica (Cuya) and kaolinite and muscovite (Kaolinite Hills). Comparison of the two datasets shows that Hyperion identifies similar minerals and produces grossly similar mineral mapping results as AVIRIS, however, it doesn't produce the level of detail available from the AVIRIS data. Some minerals are missed, and others are confused (dickite/kaolinite). This is largely the effect of reduced Hyperion signal-to-noise-performance compared to the AVIRIS (~20:1 and less for these Hyperion data, compared to >500:1 for AVIRIS) (Kruse, 2002). The Hyperion data are most useful for small-scale reconnaissance mapping and are attractive because world-wide acquisitions are possible. In the Los Menucos case, however, the problem was that no cloud-free data were acquired during the southern hemisphere summer – this would have maximized the SNR.

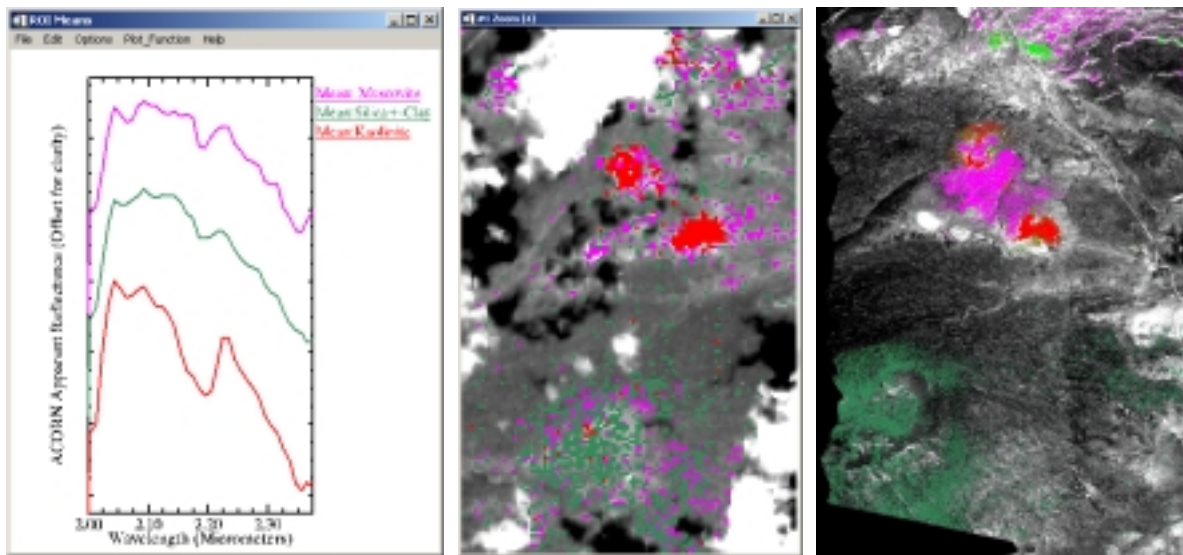


Figure 10: Left - Hyperion endmember spectra. Green is silica+mica, red is kaolinite, magenta is muscovite. Center, Hyperion grayscale image with MTMF mineral map overlay: Green is Cuya area with hydrothermal silica+mica signature. Red is Kaolinite Hills area with kaolinite signature. Magenta shows areas with muscovite signatures. White areas are clouds and dark areas are cloud shadows. Right: AVIRIS data for the same approximate area. Colors are the same as for Hyperion.

The 17 June (southern hemisphere winter) Hyperion data spectra, however are sufficiently noisy (<15:1) SWIR SNR that extraction of characteristic mineral spectra is extremely difficult. Large area averages are required make any mineral identifications and even then, only the strongest features are recognized (Figure 11).

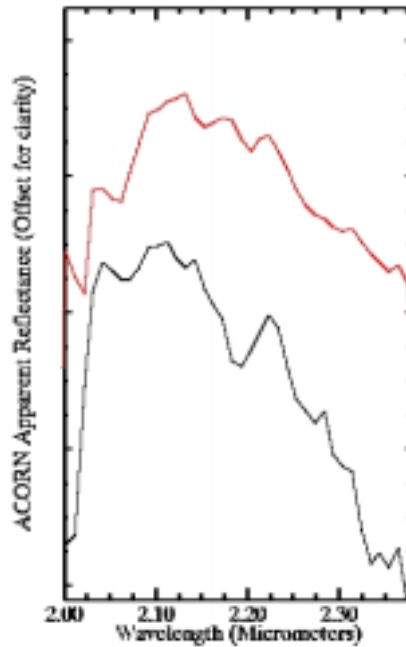


Figure 11: ACORN Hyperion apparent reflectance spectra for the Cuya site (hydrothermal silica±sericite). Black=25 February 2001, Red=17 June 2001.

The Los Menucos district provides an excellent case history of a complex epithermal gold system initially identified using satellite imagery and further mapped and explored using hyperspectral imaging systems. The AVIRIS data were very useful in this effort. Hyperion analysis and comparison to known geology derived from AVIRIS data and ancillary ground measurements generally validate in-orbit mineral mapping and Hyperion performance, however, clouds and low SNR (“winter” – low solar zenith angle) limit effectiveness. Additional summer season Hyperion data were requested for the Los Menucos sites to allow more detailed study and to broaden the scope to other AVIRIS-covered areas. These data have not been acquired as of the date of completion of this project.

Study Area Results: Cuprite, Nevada

Cuprite, Nevada, located approximately 200 km northwest of Las Vegas (Figure 12) is a relatively undisturbed acid-sulfate hydrothermal system exhibiting well exposed alteration mineralogy consisting principally of kaolinite, alunite, and hydrothermal silica. The geology and alteration were previously mapped in detail (Abrams et al., 1977; Ashley and Abrams, 1980). Swayze (1997) includes a good geologic summary, a generalized geologic map, and detailed mineral maps derived from 1990 and 1994 AVIRIS data. Cuprite, has been used as a geologic remote sensing test site since the early 1980s and many studies have been published (Goetz et al., 1985; Ashley and Abrams, 1980; Goetz. and Strivastava., 1985; Swayze., 1997; Shipman and Adams, 1987; Kruse et al., 1990; Hook, 1990; Swayze et al., 1992; Goetz and Kindel, 1996; Kruse et al, 2002a).

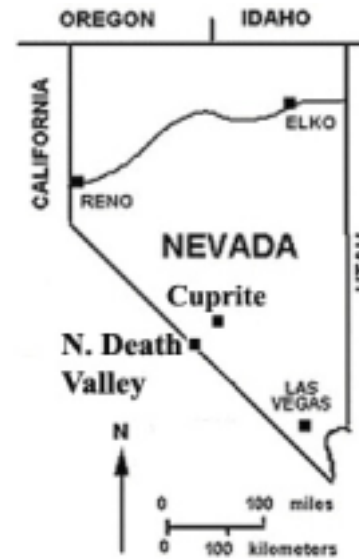


Figure 12: Location of the Cuprite and Northern Death Valley Sites.

This study compares mineral mapping results from AVIRIS data acquired 19 June 1997 to Hyperion data collected 1 March 2001. Figure 13 shows reference images for the AVIRIS and Hyperion data.

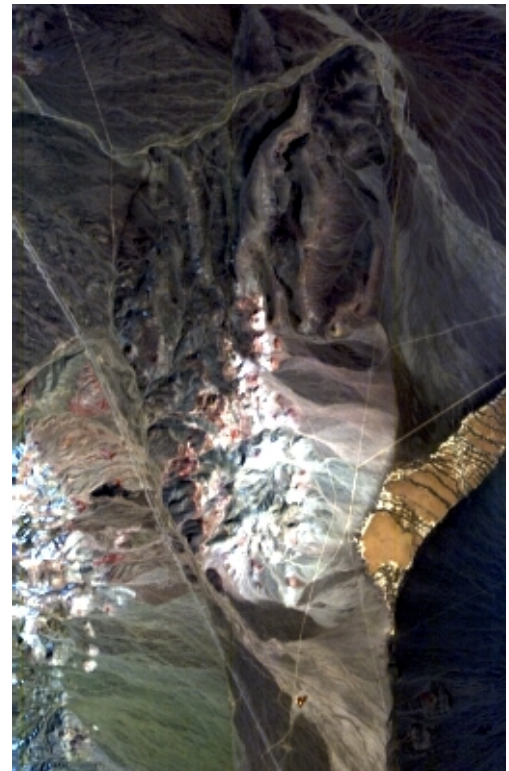
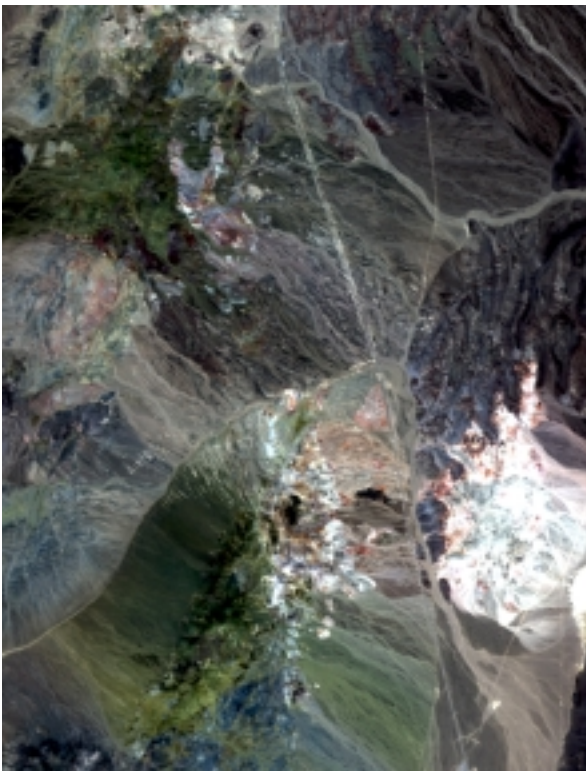


Figure 13: Reference images showing the AVIRIS (left) and Hyperion (right) coverage of the Cuprite, Nevada site. The site is typically described as consisting of two hydrothermal centers (Swayze, 1997). These can be seen in the images as bright areas to the right and left of the road running from NW to SE across the scenes.

Operationally, spectral bands covering the short wave infrared (SWIR) spectral range (2.0 – 2.5 μm for AVIRIS and 2.0 – 2.4 μm for Hyperion) were selected and these bands were linearly transformed using the MNF transformation. Figure 14 shows a plot of the MNF eigenvalues for both datasets. Higher eigenvalues generally indicate higher information content. The MNF results indicate that the AVIRIS data contain significantly more information than the Hyperion data covering approximately the same spatial area and spectral range.

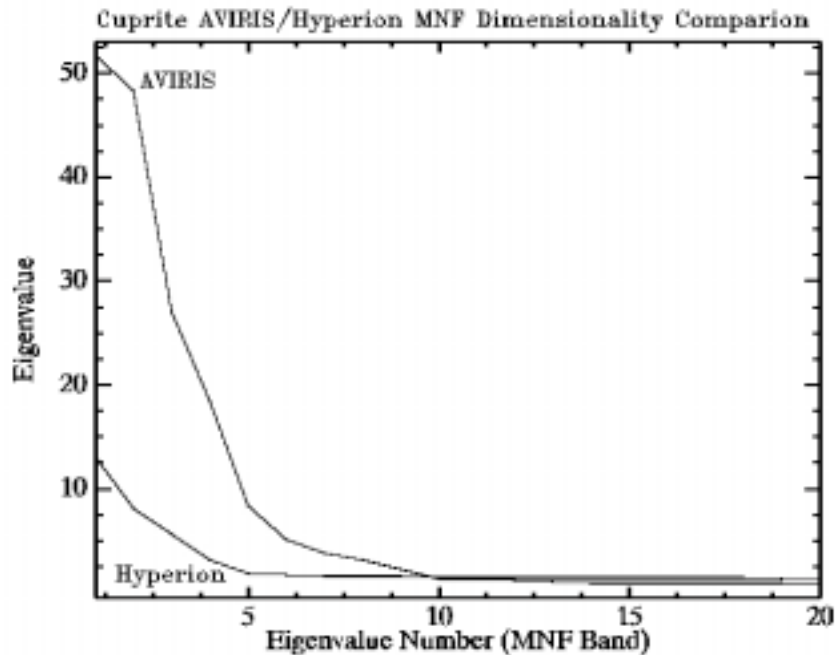


Figure 14: Comparison of AVIRIS and Hyperion eigenvalues plotted versus MNF Band. Note break in slope around 10 for AVIRIS and much lower around 5 for Hyperion.

The actual data dimensionality is usually determined by comparing both the eigenvalue plots and the MNF images for each dataset (Figures 14, 15, 16). In the case of AVIRIS, the MNF analysis indicates a dimensionality of approximately 20. The Hyperion data exhibits dimensionality of approximately 6.

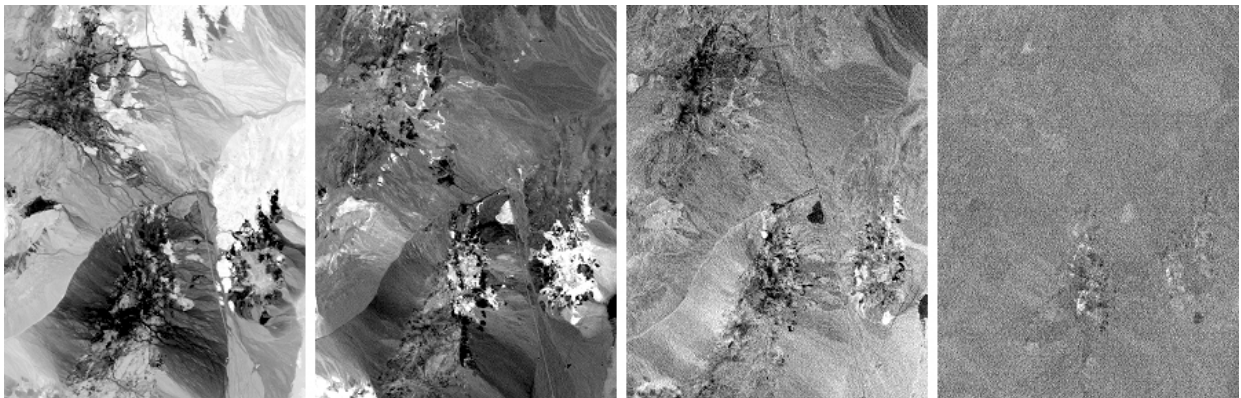


Figure 15: MNF images for the AVIRIS SWIR data. Images from left to right, MNF band 1, MNF band 5, MNF band 10, MNF band 20.

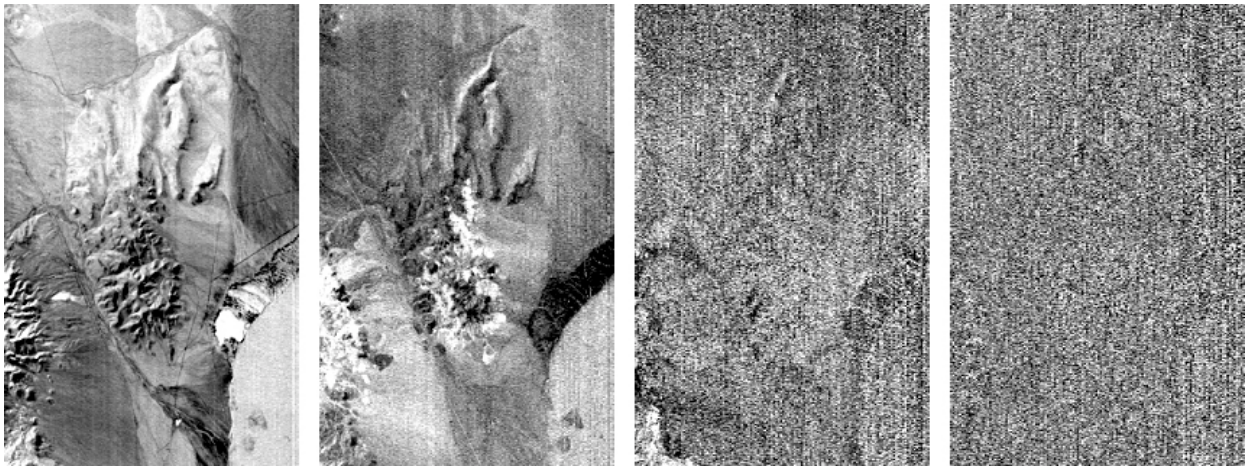


Figure 16: MNF images for the Hyperion SWIR data. Images from left to right, MNF band 1, MNF band 2, MNF band 5, MNF band 10.

The top MNF bands for each data set (20 for AVIRIS, 6 for Hyperion) were used to determine the most likely endmembers using the PPI procedure. These potential endmember spectra were analyzed using the n-dimensional scatterplot approach and unique endmember signatures extracted and exported to ROIs in the image. Mean spectra were then extracted for each ROI from the apparent reflectance data to act as endmembers for spectral mapping (Figure 17). Note that AVIRIS detected several varieties of alunite plus an additional kaolinite-group mineral (dickite) that were not detectable using the Hyperion data. These endmembers (or a subset in the case of AVIRIS) were used for subsequent classification and other processing. Mixture-Tuned-Matched Filtering (MTMF) was used to produce image-maps showing the distribution and abundance of the selected minerals. (Note: MNF endmember spectra, not reflectance spectra are used in the MTMF Results images for both AVIRIS and Hyperion were produced by correcting the Hyperion data to match the AVIRIS spatial scale and orientation as described above. Selected results were combined as color-coded images to show the distribution of the principal (spectrally predominant) minerals (Figure 18).

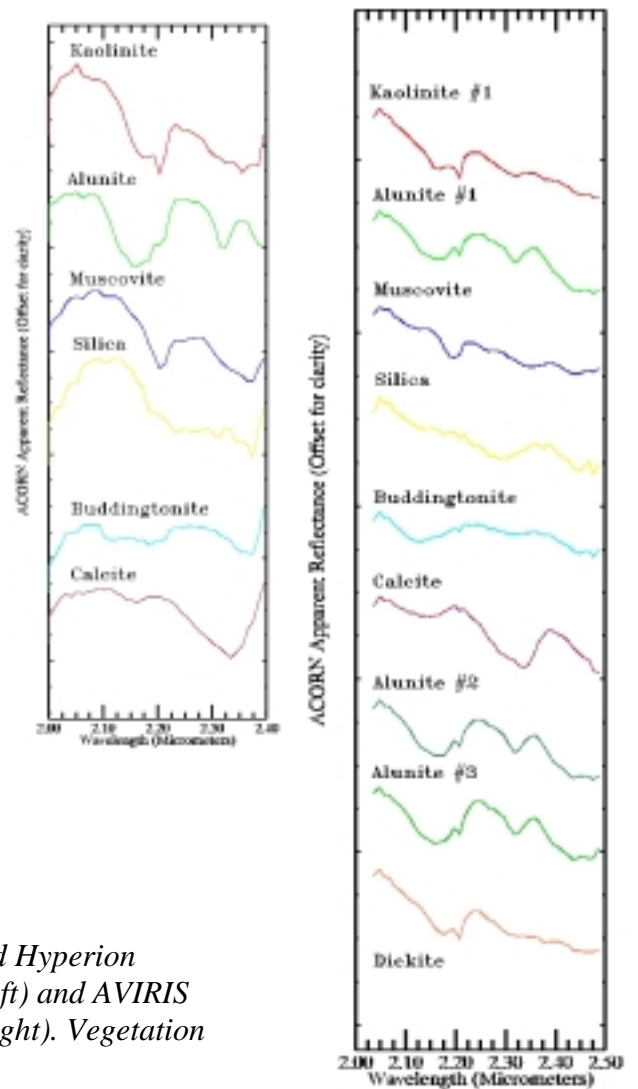


Figure 17: Comparison of selected Hyperion endmember spectra (left) and AVIRIS endmember spectra (right). Vegetation spectra not shown.

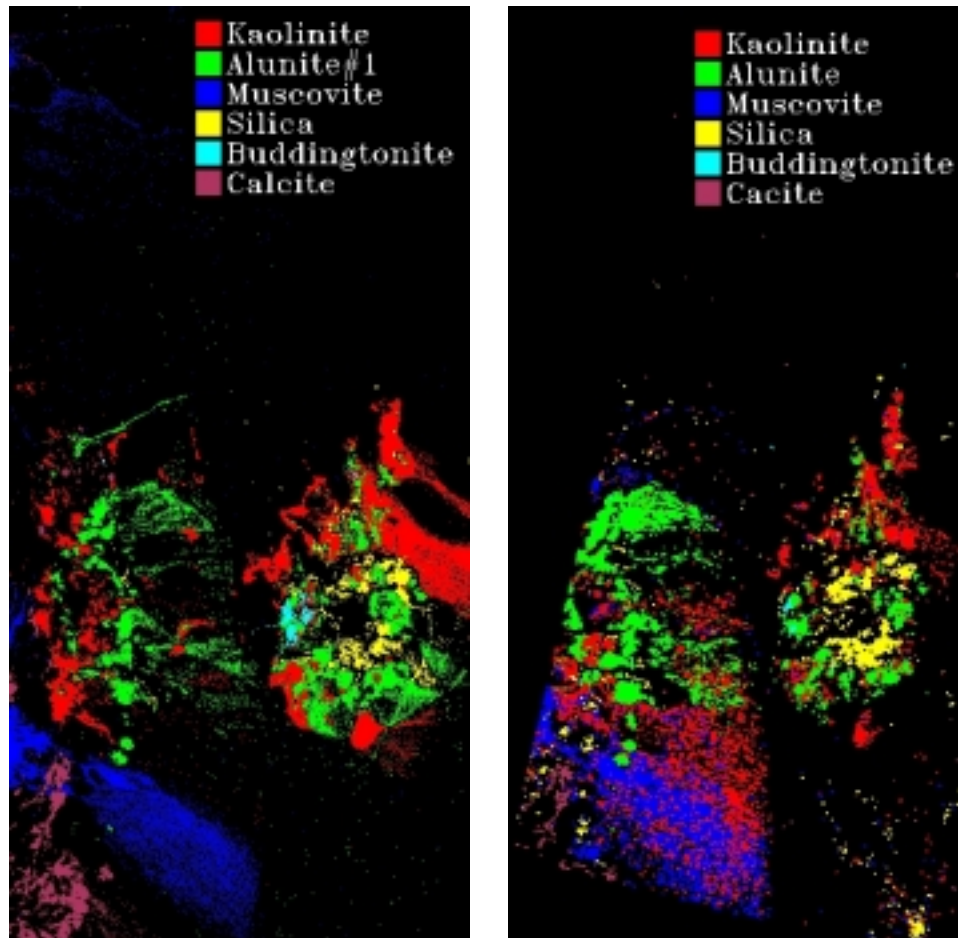


Figure 18: *MTMF mineral maps for AVIRIS (left) and Hyperion (right) produced using the endmember spectra in Figure 17.*

Visual comparison of the two classified datasets shows that Hyperion identifies similar minerals and produces similar mineral mapping results to AVIRIS. In this case, the difference in pixel size is generally inconsequential (causing only slight loss of spatial detail in Hyperion results). It seems likely that the lower SNR of the Hyperion data (calculated at approximately 25:1 for this site vs >500:1 for AVIRIS) does affect the ability to extract characteristic spectra and identify individual minerals. (See the Hyperion buddingtonite spectrum in Figure 17 above, which does not clearly show the characteristic buddingtonite spectral feature shape near 2.11 μm , which is well resolved in AVIRIS [Figure 17] and other hyperspectral aircraft data) (Kruse et al., 1990, 2000; Swayze, 1997). This spectrum could also, however, be an effect of the pixel size causing greater mixing in the Hyperion data for relatively small buddingtonite occurrences. Additionally, bear in mind that Figure 18 shows a basic AVIRIS mineral map. It is possible to extract more detailed mineralogic information from the AVIRIS data (Swayze, 1997; Green et al., 2001; Kruse et al., 2001, 2002a;) as well as abundance information (Boardman and Kruse, 1994; Boardman et al., 1995, Kruse et al., 1999). Determination of abundances for minerals identified by Hyperion is possible, but not illustrated here. Our analysis also indicates that the Cuprite Hyperion data do not allow extraction of the same level of detailed mineralogic information as AVIRIS (eg: within-species separation of micas and temperature mapping of Alunites) (Swayze, 1997; Swayze et al., 1992). Actually though, Hyperion performs surprisingly well considering the overall SWIR SNR.

Cuprite Accuracy Assessment and Error Analysis

Visual comparison of the Hyperion and AVIRIS MTMF image maps in Figure 18 using the AVIRIS data as the “Ground Truth” indicates that in general, using these mapping methods, the two datasets produce similar mapping results. Figure 19 shows a comparison of MTMF results for the minerals kaolinite and alunite, presented as binary images covering the data’s overlapping area (white is a specific mineral, black is unclassified), and it can be seen that these have similar patterns of classified pixels for the selected minerals.

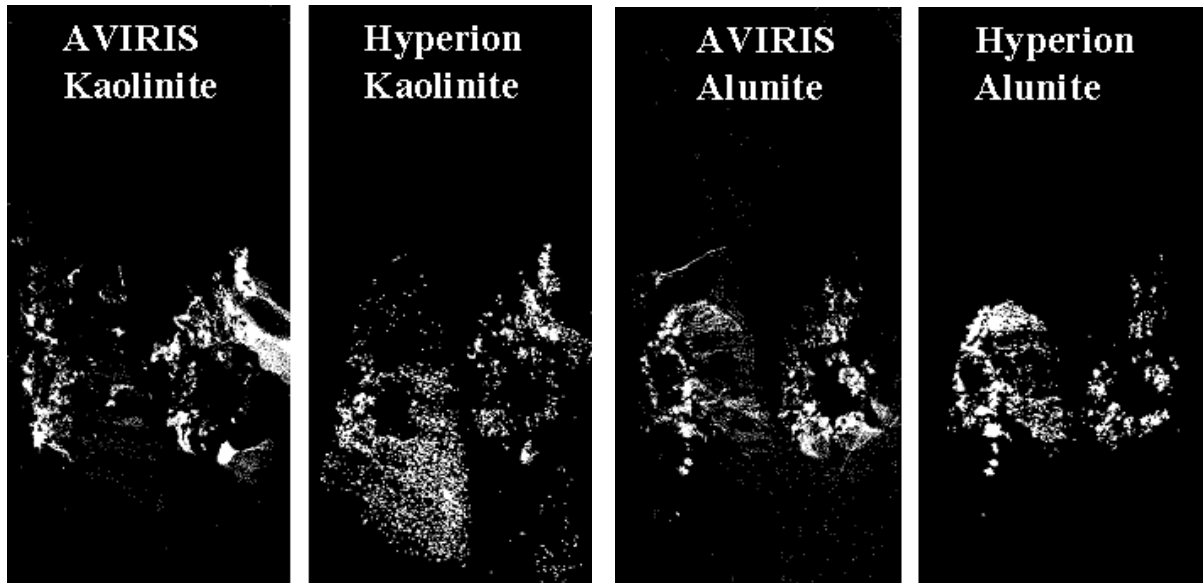


Figure 19: Comparison of MTMF mineral mapping results for kaolinite and alunite. White pixels indicate successful classification.

Detailed direct comparison of the mapping results demonstrates, however, that the correspondence is not as great as may be thought from visual comparison. Comparison of the MTMF spectral mapping results using a confusion matrix approach shows that many pixels classified using AVIRIS are unclassified on Hyperion (up to 60%, but variable by mineral). These are errors of omission. This is probably explained by the differences in SNR between the two datasets. Some spectral features are simply below the level of detection on the Hyperion data. The same analysis, but excluding the unclassified areas, yields approximately 75% overall agreement of Hyperion to AVIRIS, with a Kappa Coefficient of 0.66 (Table 3) (Richards, 1994). This highlights errors of commission (where pixels mapped as one mineral by AVIRIS are mapped as another mineral by Hyperion). First, some pixels unclassified using AVIRIS are misclassified as a specific mineral on Hyperion (around 5% commission error). Additionally, some pixels classified by AVIRIS as specific minerals are misclassified as different minerals on Hyperion (~25% commission error). Specifically, there is minor classification error between: Kaolinite mapped by Hyperion as Muscovite (7%), Kaolinite and Silica (4%), Alunite and Silica (4%), Alunite and Muscovite (1%), Muscovite mapped as Silica (1%), Muscovite and Calcite (1%), Silica and Alunite (5%), Silica and Muscovite (2%), Silica and Calcite (2%), Buddingtonite and Kaolinite (5%), Calcite and Muscovite (9%), and Calcite and Silica (4%). Moderate errors occur between: Kaolinite mapped by Hyperion as Alunite (15%), Alunite and Kaolinite (17%), and Silica and Kaolinite (11%). The highest errors occur between: Buddingtonite mapped by Hyperion as Alunite (59%), and Muscovite mapped by Hyperion as Kaolinite (25%). Table 3 summarizes the error relationships between minerals.

Table 3: Confusion Matrix comparing Hyperion MTMF mapping results to AVIRIS “Ground Truth” MTMF results.

	AVIRIS Ground Truth (Percent)						
Hyperion Class	Kaolinite %	Alunite %	Muscovite %	Silica%	Buddingtonite%	Calcite %	Total
Kaolinite	74.48	16.64	25.32	10.68	5.33	3.54	36.44
Alunite	14.28	79.86	0.06	5.39	59.17	0.00	31.47
Muscovite	7.12	0.70	72.77	2.15	0.00	9.45	20.76
Silica	3.72	2.14	1.00	80.16	0.00	6.69	8.73
Buddingtonite	0.02	0.34	0.00	0.00	35.50	0.00	0.55
Calcite	0.39	0.32	0.85	1.62	0.00	80.31	2.05
Total	100.00	100.00	100.00	100.00	100.00	100.00	100.00

While this comparison serves to highlight the accuracy and overall performance of the Hyperion dataset compared to AVIRIS, several other issues may affect the accuracy assessment. These include: 1) the data coverage (spatial extent) of the two datasets – they cover substantially the same ground, but not exactly (affects unclassified class), 2) the data pixel size (AVIRIS is 20m, Hyperion 30m), 3) Image acquisition differences (date/time, atmospheric conditions, SNR), 4) slightly different spectral characteristics (2.0 – 2.5 μm for AVIRIS vs 2.0 – 2.4 μm for Hyperion; varying band centers and spectral resolution), 5) different image-based endmembers spectra used for MTMF (endmember spectra not identical), 6) MTMF threshold consistency and class combining (AVIRIS), and 7) Hyperion to AVIRIS image registration accuracy.

Study Area Results: Virginia City, Nevada

The Comstock mining district, near Virginia City, Nevada, comprising the Comstock, Silver City, Occidental and Flowery lodes, is located 24 km SE of Reno, Nevada. Mineral deposits in the area represents a world-class low-sulfidation epithermal Au-Ag mineralization system, with the Comstock lode alone producing 312 tons of gold and 72600 tons of silver (Thompson, 1956; Vikre 1989). Extensive hydrothermal alteration products of multiple episodes have been recognized in the district. The geology, hydrothermal alteration, Au-Ag mineralization and geochronology of this area have been described by numerous workers (Whitebread 1976; Vikre *et al.* 1988; Vikre 1989 & 1998; Henkle *et al.* 1993), and are briefly summarized as follows.

Mesozoic metasedimentary, metavolcanic and granitic rocks are the oldest lithologies exposed mainly in the southern part of the district. These basement rocks are unconformably overlain by thick andesitic lava flows and breccias of the Miocene Alta Formation (20-15 Ma). The middle Miocene Kate Peak Formation (15 to 10 Ma), comprising andesitic to dacitic flows and associated dykes and stocks, overlies the Alta Formation with a slight unconformity. Dikes and stocks of the Mount Davidson granodiorite intruded the Alta Formation. The Mount Davidson granodiorite is considered co-magmatic with the Kate Peak intrusions. Siltstone, sandstone, shale, conglomerate and tuff breccia of the Coal Valley Formation overlie the Kate Peak Formation. In many places, the Coal Valley Formation is absent, and the Kate Peak Formation is overlain unconformably by the Lousetown Formation. The Lousetown Formation comprises a series of basalt and basaltic andesite flows.

Au-Ag mineralization in the Comstock mining district is hosted mainly in quartz veins and stockworks, which contain various amounts of sulfides, calcite, and adularia. Mineralization of less importance occurs in breccias and silicified zones. The mineralized veins strike predominately north $\pm 30^\circ$, except those related to the Silver City fault which run nearly east-west. Quartz-sulfides-calcite-adularia veins are hosted mainly in the Alta Formation. The age of Au-Ag mineralization in the district is 14-12 Ma, coeval with the Kate Peak volcanism. The ore-bearing volcanic rocks of the Alta and part of the Kate Peak Formations are extensively altered. Episodic hydrothermal alteration events resulted in complex and often overprinted spatial distributions of various alteration assemblages. These alteration assemblages are broadly classified into advanced argillic, argillic, propylitic, phyllic (sericitic) and silicification.

Intense and pervasive advanced argillic alteration resulted in quartz-alunite-clay assemblages, forming extensive bleached zones near Virginia City, Gold Hill, Cedar Hill, and Flowery. Alteration is commonly zoned from a quartz-alunite core, through an inner kaolin-rich clay envelope (up to a few meters thick) and an outer illite-smectite zone, to a peripheral chlorite-smectite zone. Based on radio isotopic dating and sulfur isotope compositions of alunite and observed crosscutting relations, at least part of the bleached zones were formed prior to Au-Ag mineralization in a hypogene acid sulfate alteration event probably at 17-14 Ma. Later acid sulfate alteration (12 to 9 Ma) was identified in the bleached rocks close to the north end of the mapped area, and becomes predominant further north (out of the mapped area) in the western Virginia Range.

Airborne hyperspectral reflectance data (AVIRIS) have previously proved to be very useful in identifying and mapping hydrothermal alteration zones at Virginia City (Figure 20). As part of ARIES-1 feasibility studies, simulations of ARIES-1 mineral mapping capabilities were carried out in the Comstock mining district by AIG and CSIRO using AVIRIS data (Boardman and Huntington, 1996). The simulations were focused on determining areal variations in the relative abundances of major alteration minerals, in order to clarify the details of the alteration zoning. Although the bleached zones of intense alunite-kaolin alteration at Virginia City were previously mapped (Whitebread 1976), the areal distributions of other alteration minerals (*e.g.* white micas and chlorite)

and, in particular, their abundance variations at the district scale had not been determined prior to the AVIRIS work.

Another key result of the Virginia City AVIRIS work was the verification and mapping of subtle differences in the position of diagnostic absorption features for white micas. Subtle compositional changes of these alteration minerals were used to provide valuable information on the hydrothermal alteration processes at Virginia City. The white mica identified as having short Al-OH absorption wavelength is located dominantly in the bleached rocks of the Alta and Kate Peak Formations. This white mica occurs mainly along or east of the Comstock and Silver City faults (Figure 20). The short Al-OH wavelength white mica commonly coexists with kaolin and alunite, and so belongs to the advanced argillic assemblage. The white mica with long Al-OH absorption wavelengths occurs mainly in the unbleached Alta and Kate Formations west of the Comstock and Silver City faults, and in the Mesozoic rocks in the southern part of the district (Figure 20). This long Al-OH wavelength white mica forms part of the propylitic or phyllic assemblages. The medium Al-OH wavelength white mica was mapped out mainly in the central part of the district, close to the Comstock fault between Virginia City and Gold Hill, and around the Flowery mine (Figure 20). Spatially, this white mica tends to be associated with the short rather than the long Al-OH wavelength types.

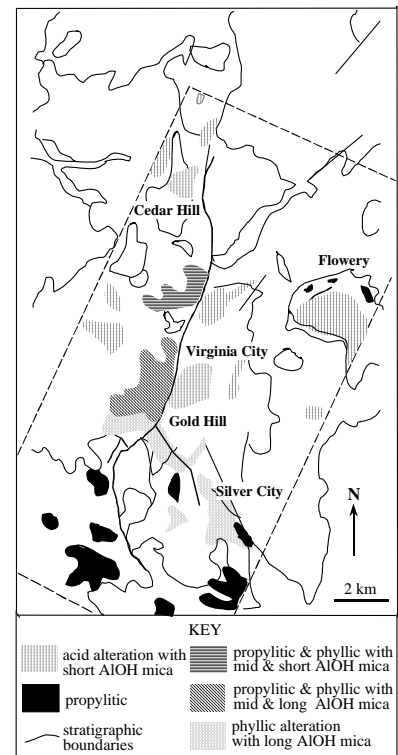


Figure 20: AVIRIS mineral mapping results for the Virginia City area, Nevada.

Hyperion data were acquired for the Virginia City site on several dates (see Table 2). The SWIR bands (2.012 – 2.4 μm) for the 2 May 2001 scene were used by CSIRO to assess Hyperion's mineral mapping capabilities. Endmembers extracted are shown in Figure 21 and mapped in Figure 22. Note that alunite was not mapped using Hyperion. This is surprising, as it is well mapped by AVIRIS. The Hyperion kaolinite mapping appears to match AVIRIS quite well, however, no dickite sub-species was found. Hyperion's capability to map the full range of illite / mica species is somewhat limited compared to AVIRIS. Only 2 varieties were located, with more limited wavelength ranges than previously mapped using AVIRIS. Note that Mg(OH) minerals (ie those with >2300 nm absorptions), such as chlorite, amphibole, epidote, carbonates) are very hard to map reliably using Hyperion, and locations only vaguely match AVIRIS results.

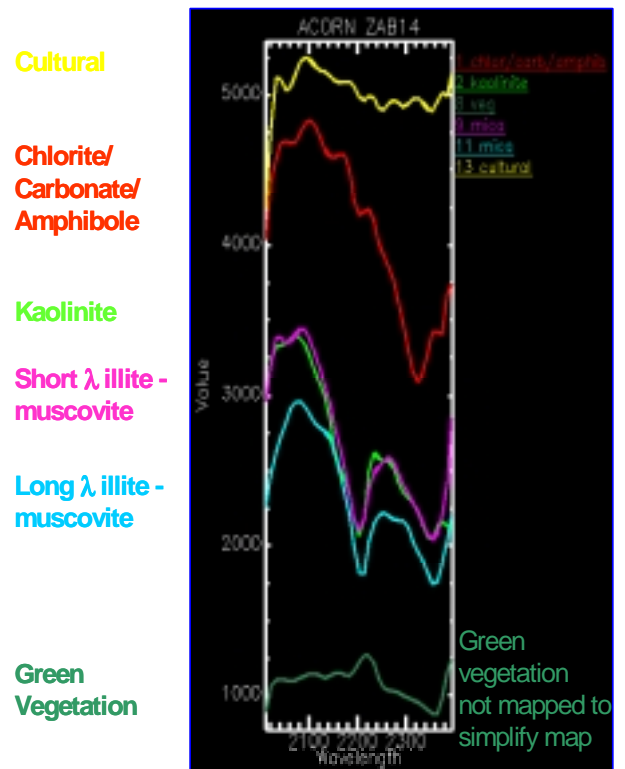


Figure 21: CSIRO Hyperion Endmembers.

The AVIRIS/Hyperion comparisons for the Virginia City site show that this Hyperion dataset is at the margin of operational utility. It appears that lower albedo, vegetated, heterogeneous, mountainous, mixed terrain leads to particularly low SNR for this scene. Consequently manual mapping methods are difficult (some minerals mapped, others missed – the 2.3 μm MgOH mineral detection severely hampered) and automatic mineral mapping methods mostly fail. While mapping success is evident in near-100% exposed, high albedo areas with little mixing and little vegetation, our conclusion is that the overall effort required for Hyperion datasets of this quality is probably too much for most operational users.

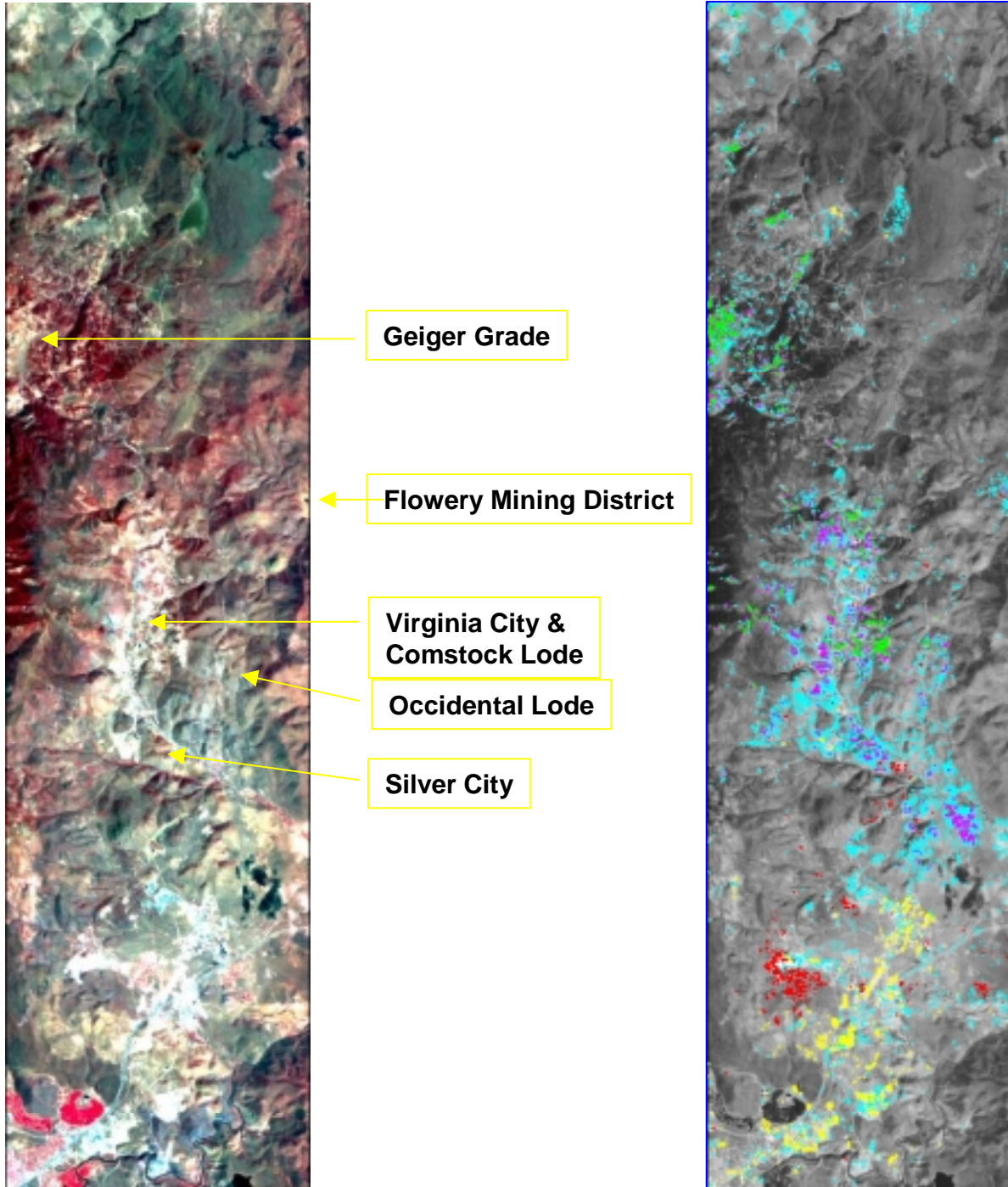


Figure 22. Left - Hyperion color IR image for the Virginia City site with key sites marked. Right - Hyperion mineral map showing distribution of minerals identified in Figure 21. Yellow=cultural, red=chlorite/carbonate/amphibole, green=kaolinite, magenta=short λ muscovite, cyan=long λ muscovite, sea green=vegetation.

Study Area Results: Steamboat Springs, Nevada

The Steamboat Springs hydrothermal system is described as a present-day equivalent of epithermal gold-silver deposits (White 1955; White 1967). This hydrothermal system, located just south of Reno, Nevada (Figure 23) is associated with four rhyolite domes, and thermal activity has probably been continuous for at least the past 0.1 m.y (Silberman et al., 1979). Numerous wells have been drilled at Steamboat for geothermal energy and to obtain hot water for local resort facilities. Wells range from 218 - 558 m with maximum measured temperature of 186 degrees C (White 1968; White 1981). The principal surface mineralogy reported at Steamboat consists of chalcedonic sinter deposits (Figures 23 and 24). Dark siliceous muds are also being deposited in the active springs and acid-leached opaline residues, kaolinite, and alunite occur in solfatarically altered granodiorite and basaltic andesite in the western part of the area (Figures 1 and 2) (Sigvaldason and White, 1962; White et al., 1964; Schoen and White 1967; Schoen et al., 1974). Significant concentrations of precious metals and related pathfinder elements occur in the Steamboat Springs sinter deposits, as chemical sediments in spring vents, and as veins at depth (White 1981). Gold was detected at the 1-2 ppm level along with anomalous Ag and As concentrations in analysis of samples from several drill holes, and small amounts of Hg has been mined from the Mercury mine at Steamboat (White et al., 1992). Deep drilling at Steamboat shows vein and alteration patterns that are indistinguishable from those of many epithermal ore deposits, containing adularia, illite, montmorillonite, and chlorite-group minerals as well as kaolinite, chalcedony, calcite, and quartz. Both stibnite and cinnabar are present near the surface, however, ore-grade concentrations of metals appear to be absent both in the near surface deposits and in the veins at depth.

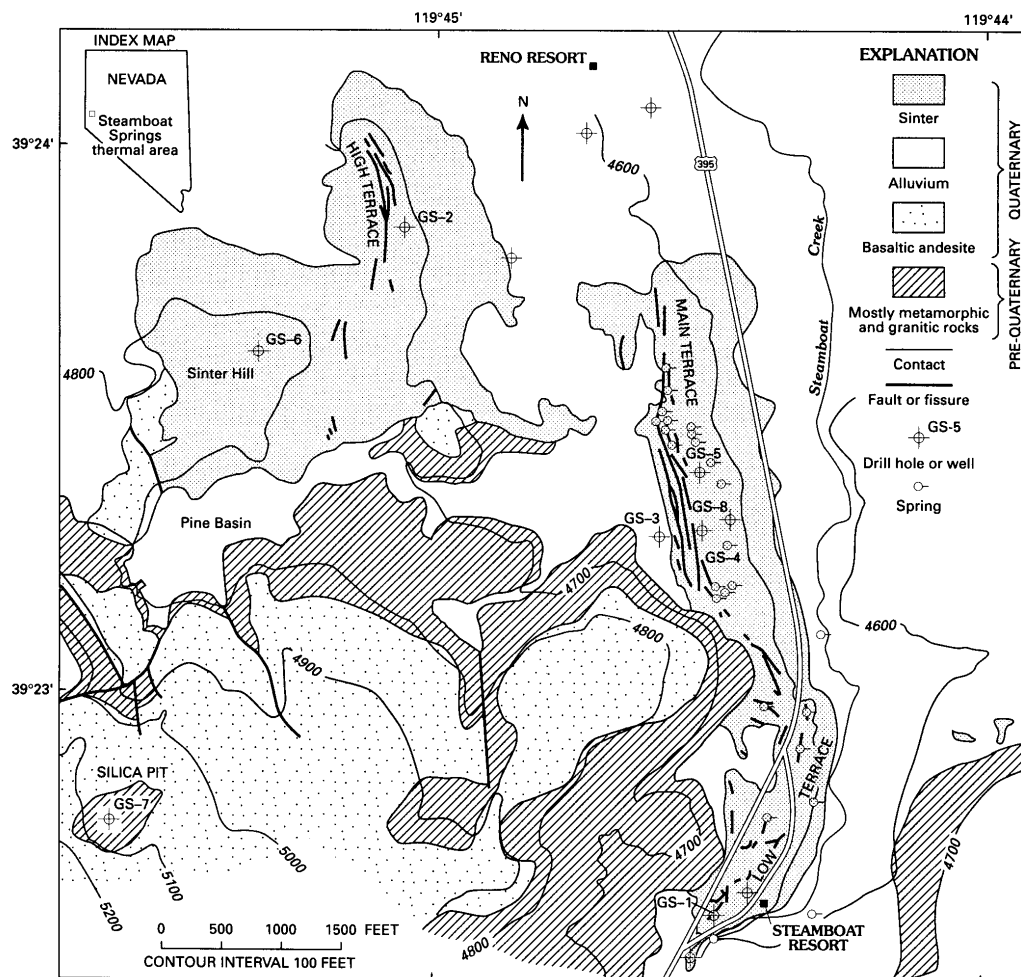


Figure 23: Location and Geology of Steamboat Springs, Nevada (from White et al., 1992)



Figure 24: Ground-level photographs at Steamboat Springs, Nevada. Left photo shows silica sinter surface. Right photo shows acid-sulfate area.

Steamboat Springs AVIRIS Results

AVIRIS data were acquired during July 1995 for the Steamboat Springs area as part of a reimbursable flight coordinated by AIG (Kruse et al., 1996a,b) and during October 1998 as part of the JPL AVIRIS low altitude test program (Chrien et al, 1999). AVIRIS data from both flights were calibrated to apparent reflectance using the ATREM method (Gao, and Goetz 1990; CSES, 1999). Data were then analyzed using standardized procedures developed by AIG (Kruse et al., 1996a,b). Figure 25 shows a color IR image and mineral map for the 1995 data (~20 meter pixels). Figure 26 shows the endmember spectra extracted from the 1995 and 1998 AVIRIS data. Figure 27 shows 1998 AVIRIS mineral mapping results.

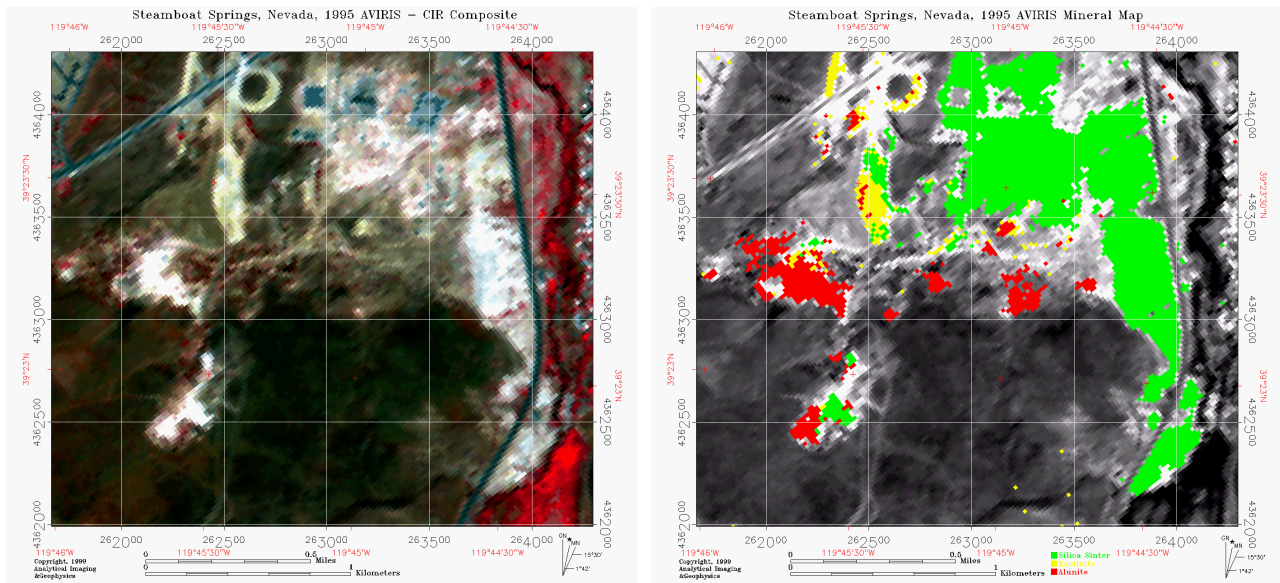


Figure 25. Steamboat Springs, NV, 1995 AVIRIS data (20m spatial resolution). Left – False color IR image. Right – AVIRIS mineral map, red=kaolinite, yellow=alunite, and green=hydrothermal silica.

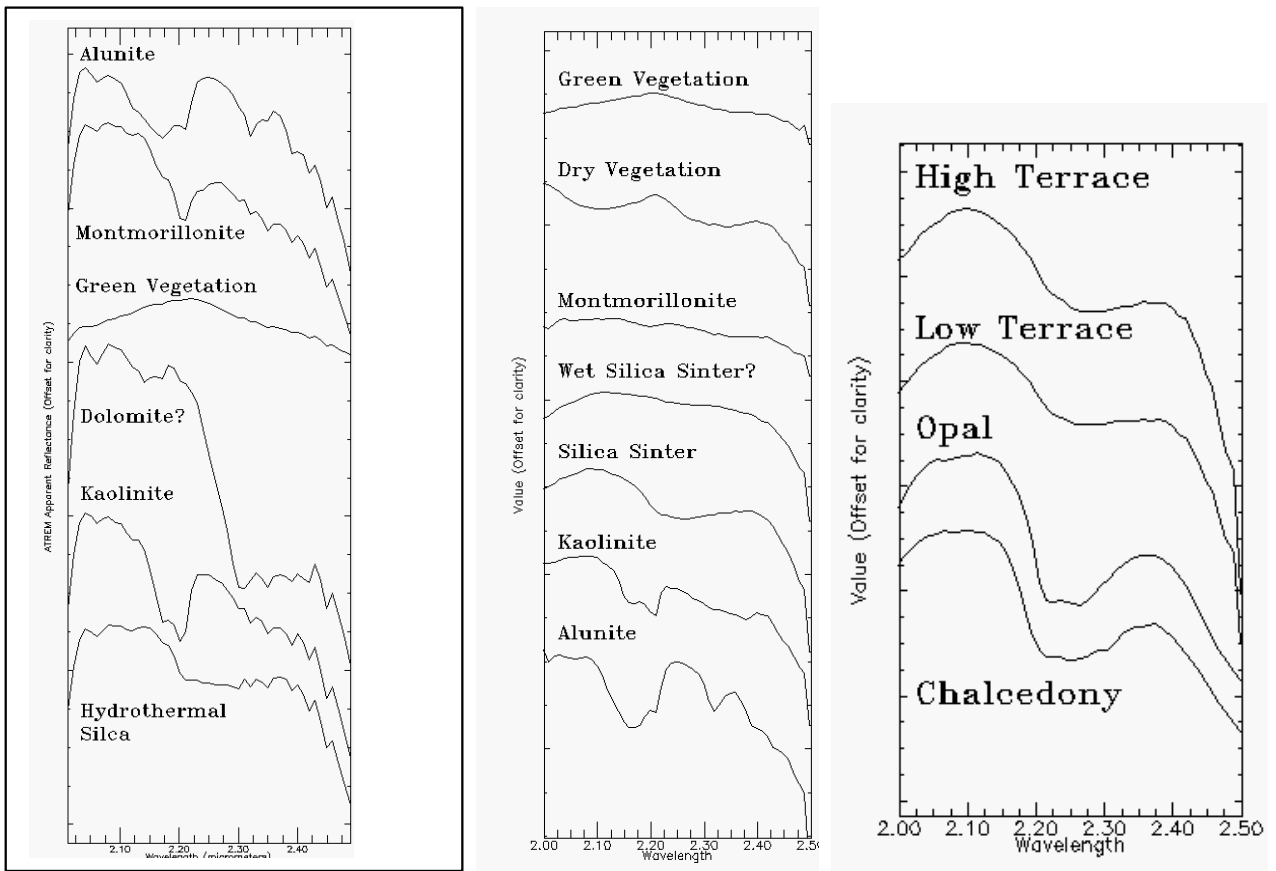


Figure 26: Left – Steamboat, NV, 1995 AVIRIS endmembers. Center - Steamboat, Nevada, 1998 AVIRIS Endmembers. Right - Comparison of active (low terrace) and inactive (high terrace) 1998 AVIRIS sinter spectra to library spectra of opal and chalcedony.

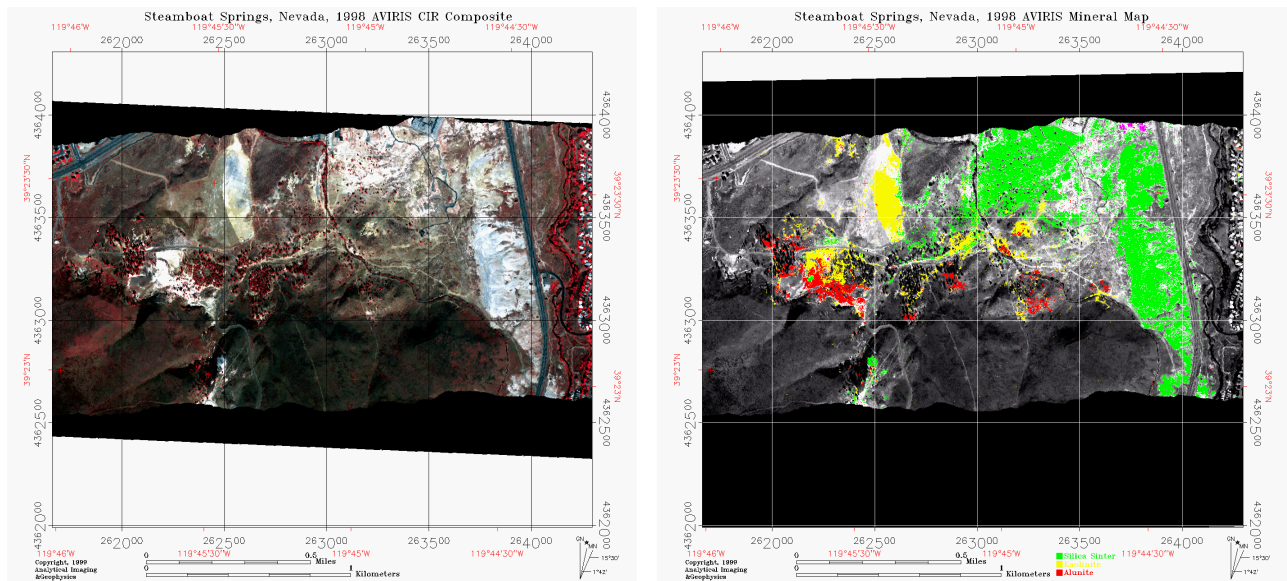


Figure 27: Steamboat Springs, NV, 1998 AVIRIS data. Left – False color IR image. Right – AVIRIS mineral map, red=kaolinite, yellow=alunite, and green=hydrothermal silica.

Both the 1995 and 1998 AVIRIS data show similar endmember mineralogies and spatial distributions. Most differences appear to be caused by the differences in spatial coverage caused by different pixel sizes. The predominant mineralogy at Steamboat Springs is the hydrothermal silica, exposed in silicious sinters. Peripheral to this are exposures of alunite and kaolinite. Montmorillonite is present, though not abundant. Both green and dry vegetation dominate outside the hot springs areas. The mapped silica distributions are apparently associated with low-lying areas (topographic lows), the “basin” and the mapped acid-sulfate areas are associated with the fringing hills and ridges. This seems to support the idea that the distribution of mineralogy at Steamboat Springs was (and still is) controlled by the current topography.

Active and inactive sinters at Steamboat Springs have been described as opal and chalcedony respectively (White et al., 1992). Spectral matching using Spectral Feature Fitting™, a least-squares band matching method (Kruse, unpublished data), however, indicates that AVIRIS spectra from both locations appear to best match an opal library spectrum. Figure 26 (right) shows a comparison of 1998 AVIRIS spectra from the active terraces (Low Terrace) and the inactive terraces (High Terrace), compared to laboratory reflectance spectra of opal and chalcedony from the USGS Denver Spectral Library (Clark et al., 1993). At first glance, the opal and chalcedony spectra appear very similar, however, slight shape differences exist between the two species. When compared with the AVIRIS spectra, these cause preferred RMS fits to the opal laboratory spectrum.

N-Dimensional scatterplotting of only the silica endmember spectra from the 1998 AVIRIS data was used in an attempt to break the silica sinter down into finer mineralogical detail. Several similar hydrothermal silica spectra were extracted from the data (Figure 28). Mixture-Tuned-Matched-Filtering was used to map the spatial distributions of materials having these subtle spectral differences. At least three of these have unique spatial distributions, as shown in Figure 28. Further field mapping and spectral measurements are required before the nature of these differences can be confirmed.

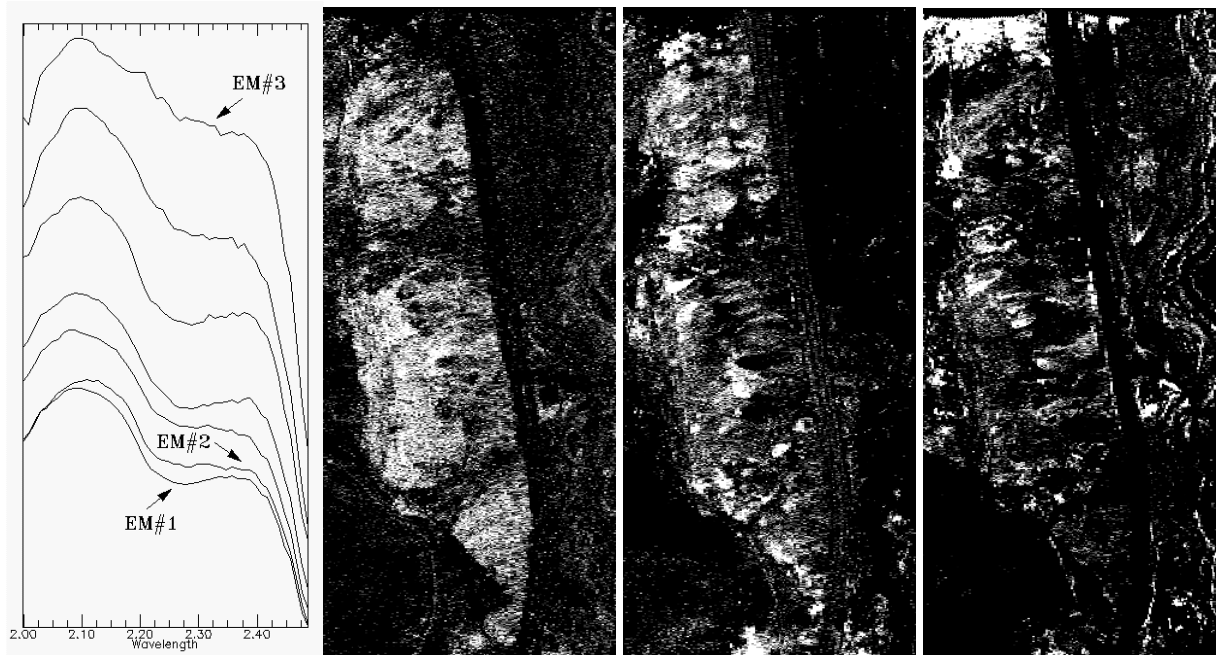


Figure 28: Spectral plots and Matched Filter images showing subtle spectral differences in 1998 AVIRIS data of the silica sinter at Steamboat Springs, Nevada. Plot shows endmember spectra. Three MF images show best matches to three distinct spatial occurrences, EM#1 (left), EM#2 (center), and EM#3 (right). Bright pixels in MF images represent best matches.

Steamboat Springs, Hyperion Results

Hyperion data acquired 22 August, 2001 were used for this analysis. The data were processed using the standard AIG/CSIRO methods, correction to reflectance; MNF, PPI, n-d visualization, spectral identification, MTMF mapping. SWIR signal-to-noise was calculated as approximately 30:1 using the mean/standard deviation method. Endmembers corresponding to alunite, kaolinite, and two varieties of silica were extracted from the data (Figure 29). Both green and dry vegetation were also identified and mapped, but are not shown. Spectral variability was observed within active and inactive sinter terraces using both AVIRIS and Hyperion data and may correspond to the difference between Opal versus Chalcedony. This, however, remains to be confirmed.

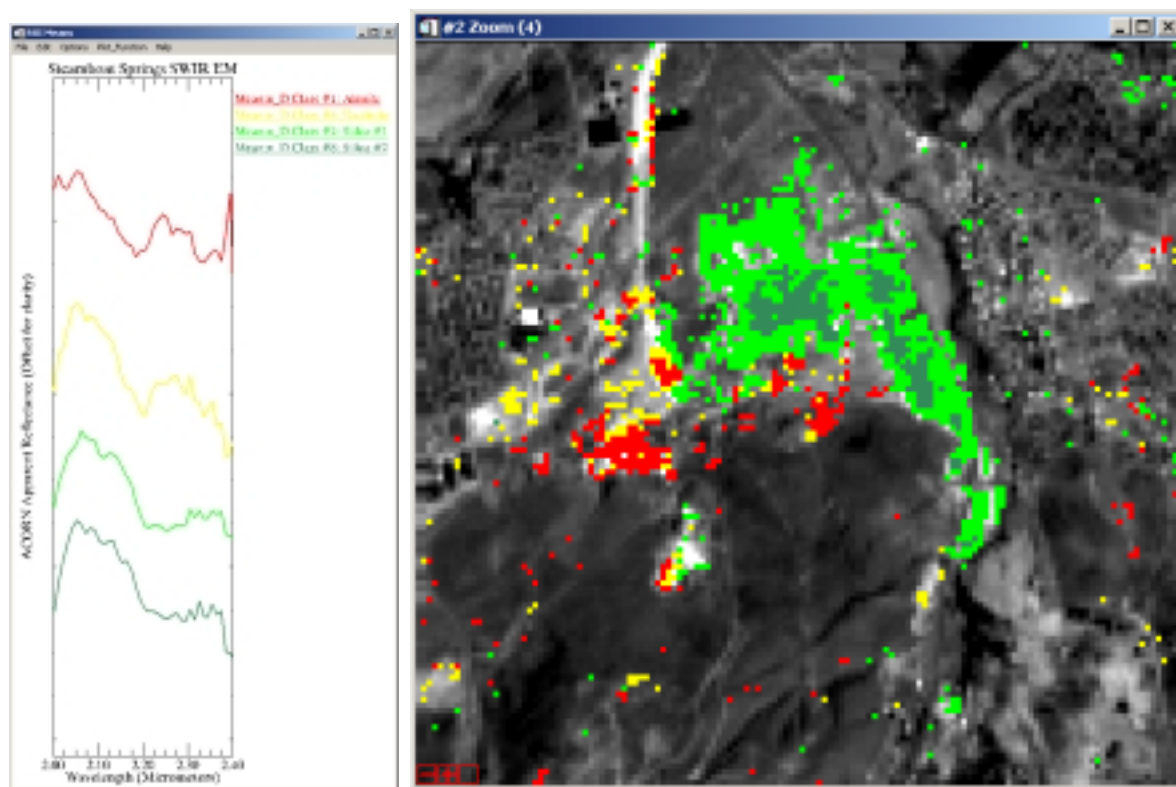


Figure 29: Steamboat Springs, NV, Hyperion endmember spectra (left) and MTMF mineral mapping results (right). Red=alunite, yellow=kaolinite, green=silica #1, sea green=silica #2.

The Steamboat Springs case history validates Hyperion data for characterizing active and fossil hot springs systems and acts as another demonstration the viability of satellite hyperspectral data for mineral mapping. At the reconnaissance level, 1995 and 1998 AVIRIS and Hyperion data produced similar results. The major minerals were detected and mapped. The AVIRIS and Hyperion data allow detailed mapping of the hot-springs-associated alteration mineralogy, including the distribution of the siliceous sinter based on an absorption feature near 2.25 μm . At Steamboat Springs, silica was mapped in terrace-like spatial patterns associated with known hydrothermal activity as well as on inactive terraces. AVIRIS data confirms Steamboat Springs as principally an alkaline hot-springs environment. Reported distributions of opal on active terraces, and chalcedony on inactive terraces, however, was not confirmed. The AVIRIS data indicate that all of the exposed silica is opaline. The 1998 low-altitude AVIRIS, with 2.4 meter spatial resolution, not surprisingly allows mapping of greater detail at the “deposit” level - “improved photo-interpretation” of spectral results. Spectral variability was observed and mapped within the active sinter terraces utilizing the 1998 AVIRIS data and the Hyperion data, however, the physical nature/cause is presently not

known. An association was noted at Steamboat Springs between the hot-springs mineralogy and the topography, with the silica sinters located principally in the basins, and the acid-sulfate minerals along positive topographic features (ridges and hilltops) along the periphery of the basin. Continued studies of a variety of hot springs using hyperspectral data will allow improved understanding of the link between active hot springs and the expression of fossil hot springs in the geologic record. Selected systems will be used to develop an operational exploration strategy utilizing integrated remote sensing for discovery and characterization of epithermal mineral deposits.

Study Area Results: Oatman, Arizona

The Oatman Mining District lies approximately 160 km southeast of Las Vegas, Nevada, mid-way between Needles, California and Kingman, Arizona. The district is about 21 miles long and 7 miles wide and is situated within the Tertiary volcanics of the Black Mountains. Elevation ranges from 670 to 820 meters above sea level.

Gold was first discovered at Oatman in 1863 in the Moss Vein and subsequent finds in other locations (Gold Road Vein, Tom Reid Vein) led to the development of a town of 10,000 at Oatman after about 1916. Production ceased in the district in 1942 after producing some 2.2 million ounces of gold and 0.8 million ounces of silver. A total of 3.8 million tons of ore averaging 0.58 ounces/ton gold and 0.17 ounces/ton silver were extracted from eight orebodies and a number of lesser deposits between 1897 and 1942.

The regional geology consists of a thick sequence of Tertiary sub-alkaline, intermediate, and silicic volcanic rocks which have been intruded by two epizonal plutons. The Black Mountains are a typical basin and Range, fault-bounded, Tertiary volcanic sequence composed of trachyte, latite, rhyolite, and basalt (Thorson, 1971; Clifton et al., 1980). Oatman lies at the center of a volcanic complex which contains at least one resurgent caldera. The orebodies are typically low sulphur, epithermal, quartz-calcite +/- adularia lode deposits. Ore deposition has occurred in diatremite zones on faults which radiate from a common point within the complex. The Tertiary volcanics rest on a Precambrian basement of schists, gneiss, and granite and are intruded by both the Times Porphyry, a granophyre laccolith, and an epizonal quartz monzonite pluton, the Moss Porphyry.

An intense and pervasive argillic alteration is evident in the center of the study area. Studies by Clifton et al. (1980) indicate that the argillic alteration is centered around a previously unmapped rhyolite center. This event was most likely responsible for the bold mineralization in the district. There are four distinct alteration assemblages at Oatman which may be directly or indirectly related to mineralization. These are:

1. pervasive argillic alteration that is characterized by the formation of alunite and sericite (muscovite) and is present in the two intrusions and intruded formations.
2. spatially restricted, phyllic wall rock alteration which is characterized by the presence of illite and has been mapped in the Tertiary volcanics. This alteration extends above the orebodies to the surface in the central district and may coalesce with zones from adjacent veins to form a wider, potentially more visible surface signature;
3. propylitic alteration which introduces chlorite, calcite, and epidote into the wall rock;
4. silicification of the wall rock characterized by the introduction of quartz along microfractures.

Oatman, AZ, AVIRIS Results

The above assemblages provide an excellent reference against which to compare and judge the Hyperion mineralogical mapping capabilities. Extensive hyperspectral mapping has been done at Oatman using AVIRIS data, and ARIES simulations have been conducted at the same 30 m pixel size that Hyperion provides (Figures 30, 31, 32, 33). There is a tremendous amount of ground truth available as well as map-referenced mineral abundance products derived from the AVIRIS and ARIES simulations. Some of the rocks at Oatman present a challenge to Hyperion for mineral detection and mapping. The propylitic alteration zone described above typically occurs in dark rocks and provides a realistic test of the SNR performance with respect to mineral identification and mapping using Hyperion.

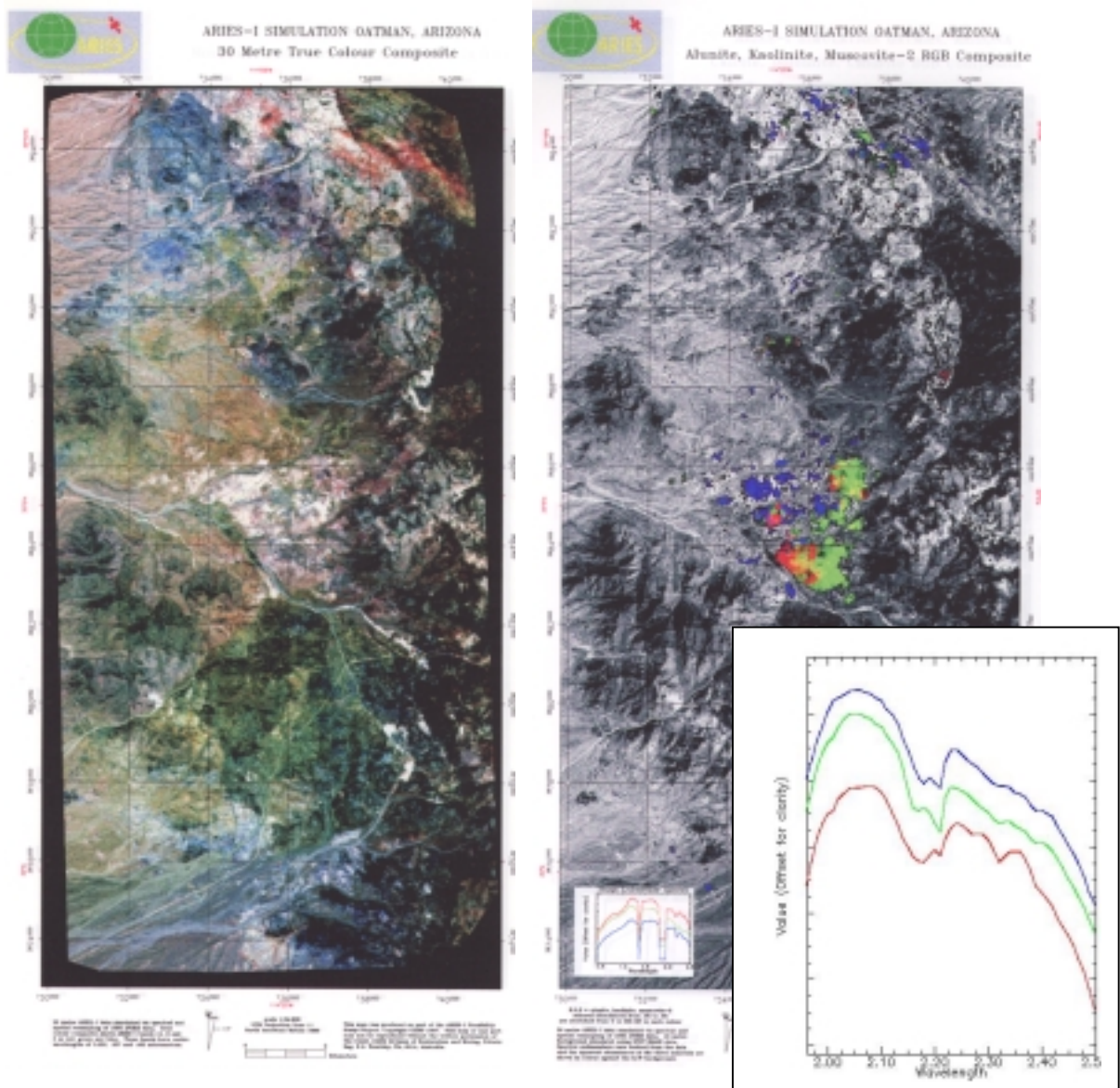


Figure 30: ARIES simulated data for Oatman Arizona. Left, true color composite; right, mineral mapping result for Alunite, Kaolinite, Muscovite 2 (RGB). AVIRIS endmember spectra are shown with same color coding. Excellent detection and mapping of alunite, kaolinite and dickite and their in-field mixtures (Note the non-primary colors).

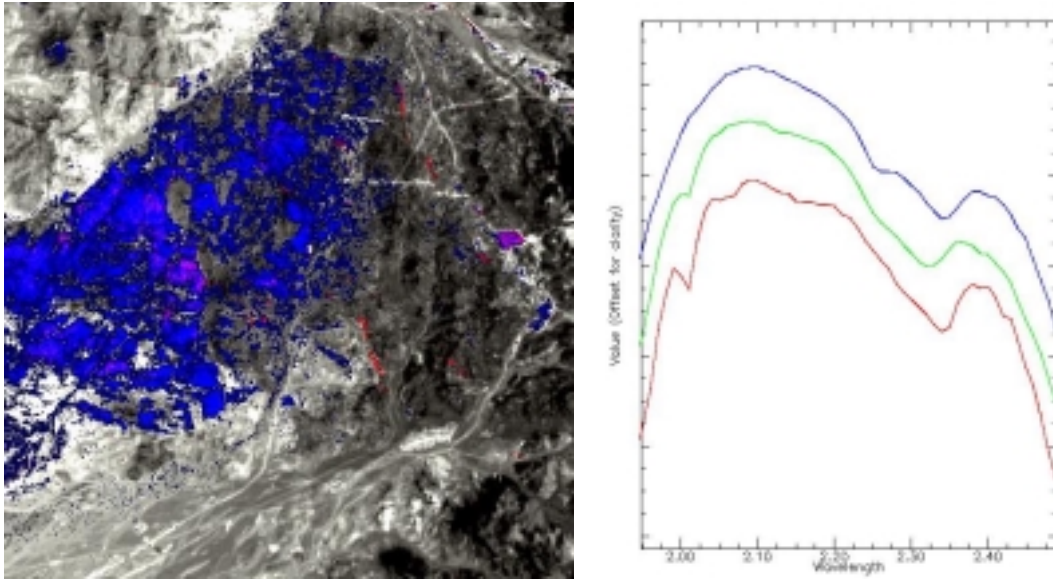


Figure 31: AVIRIS 2000 results – Carbonates vs MgOH. Left, mineral map with calcite, dolomite, and chlorite/epidote as R,G,B. Note excellent detection and mapping of calcite, dolomite and chlorite/epidote, despite subtle distinctions and sub-pixel exposures. Right, image-derived AVIRIS endmembers

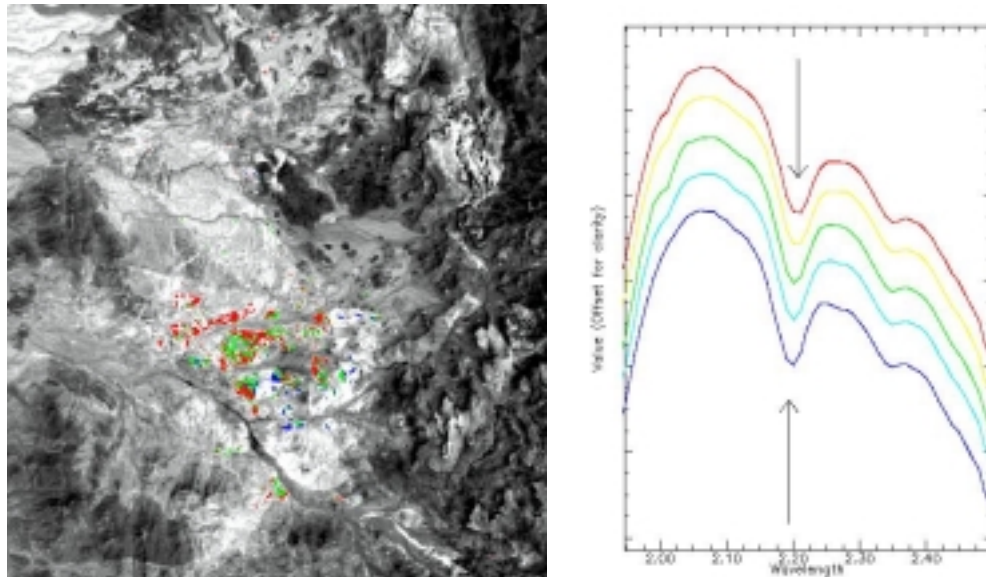


Figure 32: AVIRIS 2000 results – Mica variability (Al substitution). Full solid solution series of muscovite detected, mapped and field/lab validated w/ CSIRO. Left, mineral map showing distribution of mica with specific wavelength centers. Change of colors from red to blue corresponds with shift of main mica absorption band center near 2.2 μm to shorter wavelengths (an ~ 12 nm shift associated with cation substitution of Fe and Al). Right – AVIRIS mica endmember spectra using same color-coding.

Oatman, AZ, Hyperion Results

At Oatman, using data acquired 6 May 2001, Hyperion successfully maps basic mineralogy (kaolinite, alunite, chlorite and muscovites) (Figure 33)). Hyperion also detects and maps mineral subspecies (cation substitution) of muscovites (Figure 34). We were unable, however, to fully separate calcite from chlorite and did not detect dolomite or dickite (SNR issues) (Figure 35).

Comparison of AVIRIS MNF bands with Hyperion MNF bands reveals the main difference between the data – that of SNR performance. The Oatman AVIRIS data show a dimensionality of greater than 15, whereas the Hyperion data exhibit dimensionality on the order of 6. This can be seen in the images shown in Figure 36, where Hyperion data are dominated by noise beyond approximately 6 MNF bands. Hyperion image uniformity (striping) and relatively low SNR limit the data utility.

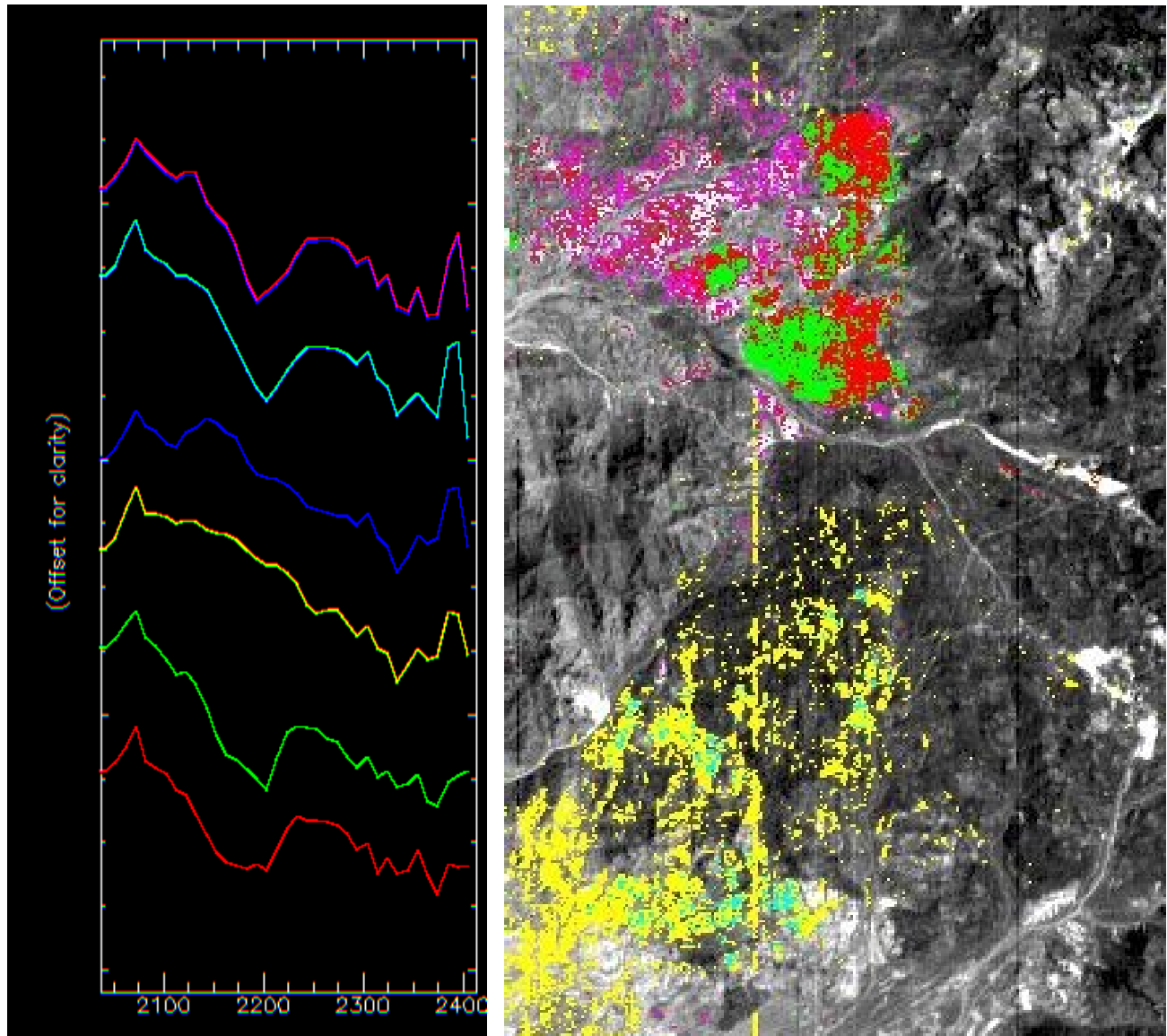


Figure 33: Hyperion combined mineral mapping. Left, Hyperion endmember spectra - Alunite = red, Kaolinite= green, chlorite/epidote = yellow, calcite = blue, lw muscovite =cyan, sw muscovite = magenta. Right, Hyperion mineral map – Note slightly different color scheme. Kaolinite = red, alunite = green, chlorite/epidote = yellow, calcite = cyan, lw muscovite =magenta, sw muscovite = maroon. Comparison to AVIRIS indicates good mapping of alunite, kaolinite, chlorite/epidote and muscovites, but poor discrimination of calcite vs chlorite/epidote along with moderate separation of muscovite subspecies.

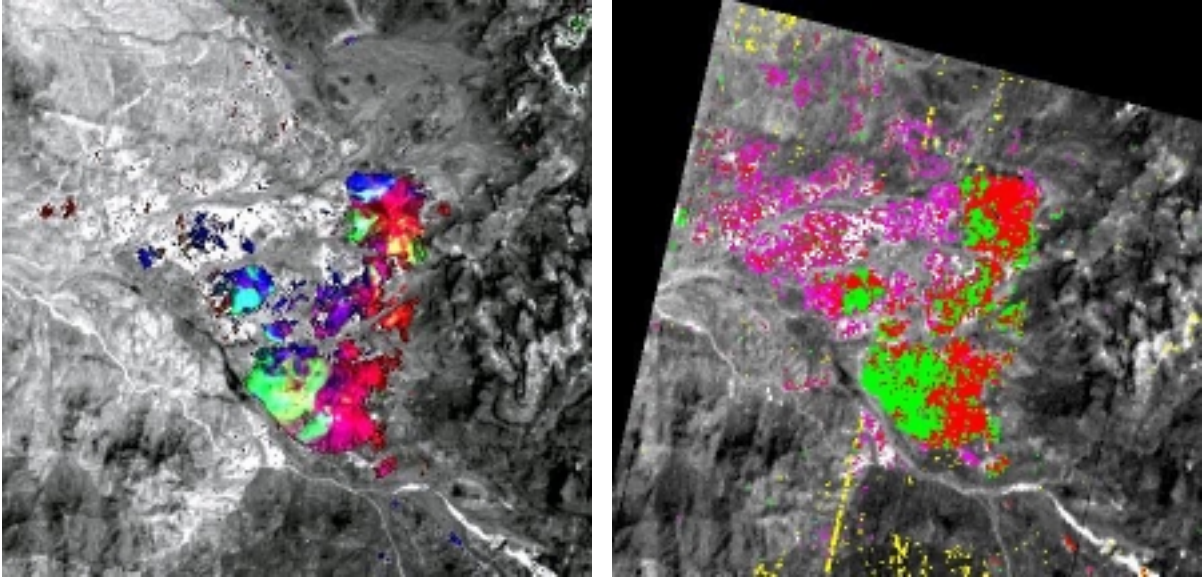


Figure 34: Left, AVIRIS RGB image showing kaolinite/alunite/dickite abundances. Right - Hyperion red=kaolinite, green=alunite, magenta/maroon = muscovite. Hyperion fails to find dickite but maps alunite and kaolinite.

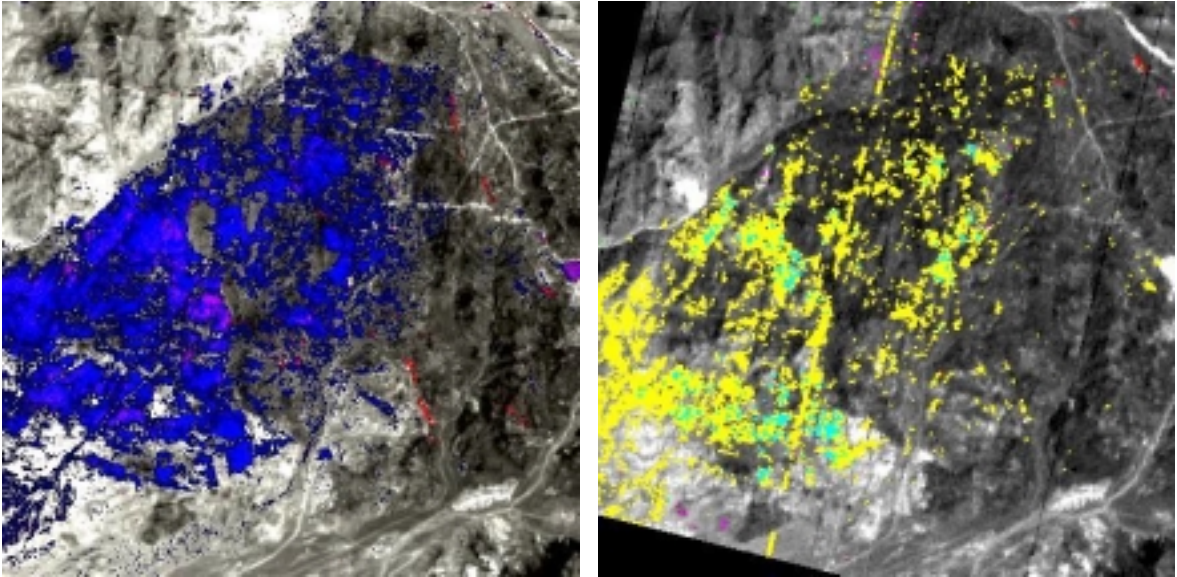


Figure 35: Left, AVIRIS RGB image showing calcite/dolomite/chlorite abundances. Right, Hyperion yellow=chlorite, cyan=calcite. Hyperion fails to find dolomite, maps chlorite well, but tends to confuse calcite and chlorite

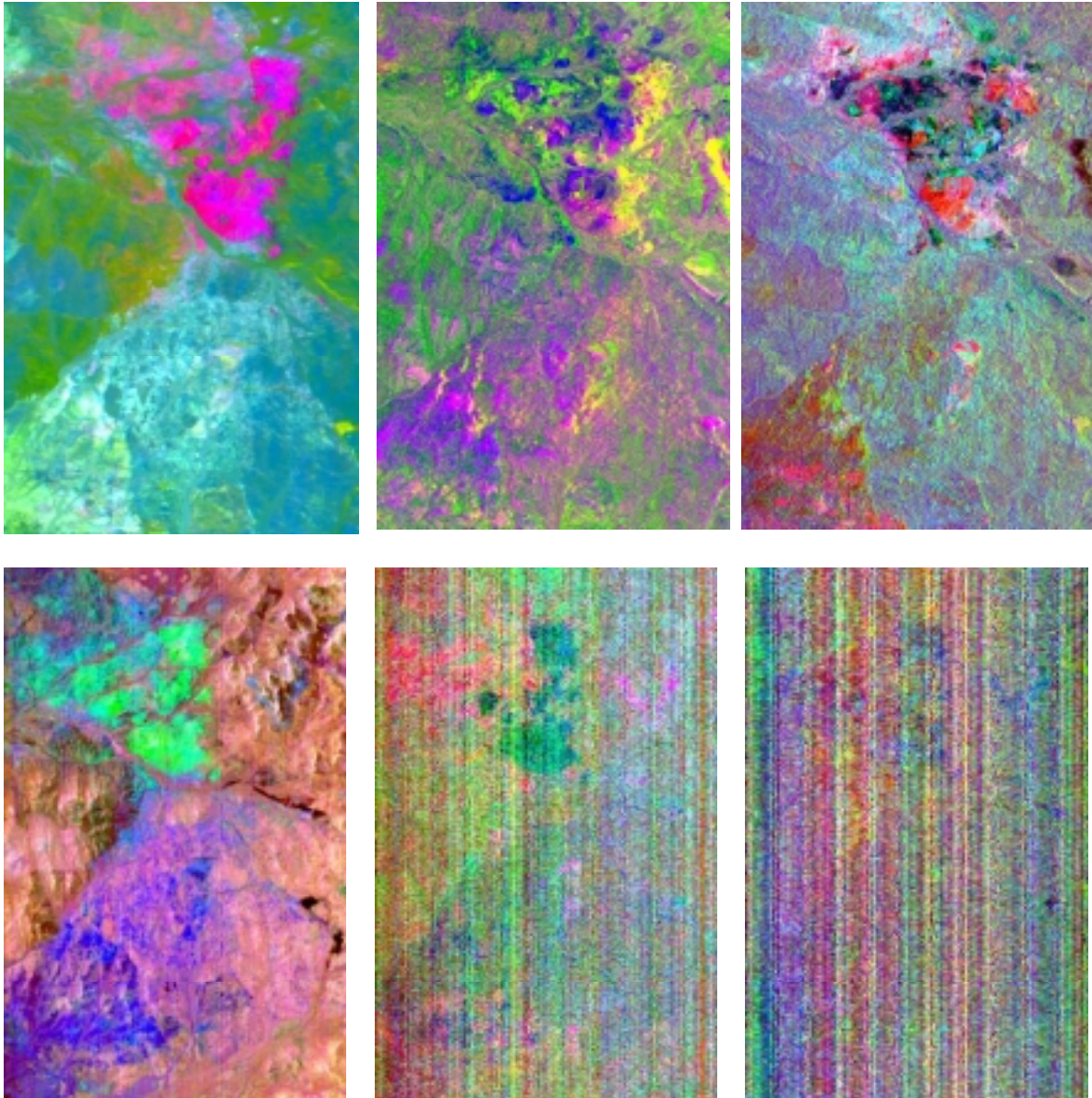


Figure 36: Comparison of AVIRIS and Hyperion MNF images. Top- RGB images of AVIRIS MNF bands 1, 2, 3; MNF bands 7, 8, 9; and MNF bands 12, 13, 14. Bottom – RGB images of Hyperion MNF bands 1, 2, 3; MNF bands 4, 5, 6; and MNF bands 7, 8, 9.

In summary, at Oatman AZ, hyperion performs about as expected, similar to AVIRIS during its 1991 collection season. Similar spectral endmembers were extracted from the Hyperion data as for AVIRIS and HyMap, but possibly only because of a priori knowledge. Hyperion successfully maps and performs basic mineralogical mapping of kaolinite, alunite, chlorite and muscovites (not possible with LANDSAT-class data). Hyperion was unable to fully separate calcite from chlorite and did not detect dolomite or dickite (SNR issues). Several sub-species of muscovites are detected and mapped with Hyperion, however, SNR/stripping limit coherent mapping. Hyperion image uniformity and relatively low SNR limit the data utility.

Study Area Results: Northern Death Valley, California/Nevada

The northern Grapevine Mountains (NGM) site, located in south-central Nevada (see Figure 12), was designated part of a U.S. Geological Survey Wilderness Study Area in 1982. It is now part of Death Valley National Park. The USGS was charged with evaluating the economic mineral potential of the area by characterizing the surface geology, alteration, geologic structure, and existing prospects and claims. Remote sensing technology available at the time (Landsat MSS and TM data) was also used as part of this evaluation. Based on alteration mineralogy at the site, an airborne survey using Geophysical and Environmental Research's (GER's) 64 channel airborne spectral profiler was also flown. Results from the remote sensing analysis, field mapping and field spectral measurements, laboratory analyses, and ancillary data led to removal of the site from consideration as a WSA in 1984 (Wrucke et al., 1984).

Because the site was relatively well understood and mapped, repeated overflights of the NGM site with a variety of remote sensing instruments were arranged from 1984 through 1998 to evaluate remote sensing technology for resource assessment and to develop advanced analysis methodologies. Remote Sensing data available for the NGM site include Landsat MSS and TM, Thermal Infrared Multispectral Scanner (TIMS), JPL Airborne Synthetic Aperture Radar (AIRSAR) and SIR-C. Imaging spectrometer (hyperspectral) data flown for the NGM site include GER Spectral Profiler (1982), Airborne Imaging Spectrometer (AIS) (1984 - 1986), Airborne Visible/Infrared Imaging Spectrometer (AVIRIS) (1987, 1989, 1992, 1994, 1995), and Low Altitude AVIRIS (1998).

The site has been studied in detail using field mapping and the remote sensing data sets described above (Kruse, 1988, Kruse et al., 1993a; Kruse et al., 1999). Precambrian bedrock in the NGM area consists of limestones, dolomites, sandstones and their contact metamorphic equivalents. Mesozoic plutonic rocks are mapped primarily as granitic-composition and some age-dates are available (Albers and Stewart, 1972). Mesozoic units mapped in the field include quartz syenite, a quartz monzonite porphyry stock, quartz monzonite dikes, and a granite intrusion (Kruse, 1987). These rocks are cut by narrow north-trending mineralized shear zones containing sericite (fine grained muscovite or illite) and iron oxide minerals (Wrucke et al., 1984; Kruse, 1987). Slightly broader northwest-trending zones of disseminated quartz, pyrite, sericite, chalcopyrite, and fluorite mineralization (QSP alteration) \pm goethite occur in the quartz monzonite porphyry. This type of alteration is spatially associated with fine-grained quartz monzonite dikes (Kruse, 1987). There are several small areas of quartz stockwork (silica flooding of the rocks) exposed at the surface in the center of the area. Skarn, composed mainly of brown andradite garnet intergrown with calcite, epidote, and tremolite, occurs around the perimeter of the quartz monzonite stock in Precambrian rocks. The NGM area has many of the characteristics common to porphyry copper deposits, however, there has not been any secondary (supergene) enrichment, and thus economic concentrations of ore do not occur. Complexly faulted, Tertiary volcanic rocks related to the Timber Mountain Caldera in southern Nevada are abundant around the southern periphery of the study area and are overlain by volcanoclastic sedimentary rocks interbedded with rhyolite and basalt (Wrucke et al., 1984). Quaternary deposits include Holocene and Pleistocene fanglomerates, pediment gravels, and alluvium; these have been mapped in reconnaissance (Moring, 1986) but no linked bedrock/surficial geology studies have been completed.

This site represents an ideal area for evaluation, validation, and demonstration of the Hyperion hyperspectral sensor. The geology is complex, but relatively well understood, the PI is very familiar with the site, and detailed field and remote sensing results are available and published (Kruse, 1988; Kruse et al., 1993a; Kruse et al., 1999). The Hyperion instrument was compared against detailed geologic maps, other multispectral and hyperspectral sensors, and numerous field and laboratory spectral measurements.

Northern Death Valley AVIRIS/Hyperion Mineral Mapping

For the purposes of this study, AVIRIS data collected 9 June 2000 (f000609t01p03_r04) were compared to Hyperion data collected July 23 2001 (EO12001204_20AD20AC_r1_PF1_01.L1_A). The Hyperion SNR was calculated using the Mean/Standard Deviation method for Racetrack Playa at ~60:1 (Best Hyperion Data Set Received at AIG). A spectral subset of bands covering the short wave infrared (SWIR) spectral range (2.0 – 2.5 μm for AVIRIS and 2.0 – 2.4 μm for Hyperion) was selected and these bands were linearly transformed using the MNF transformation. A plot of eigenvalues versus MNF band number (not shown) shows a sharp falloff in eigenvalue magnitude between 1 and 20 for AVIRIS and between 1 and 10 for Hyperion. Because higher eigenvalues generally indicate higher information content, this indicates that the AVIRIS data contain significantly more information. The actual data dimensionality is usually determined by comparing both the eigenvalue plots and the MNF images for each dataset (Figures 37 and 38). In the case of AVIRIS, the MNF analysis indicates a dimensionality of approximately 20. The Hyperion data exhibits dimensionality of approximately 8.

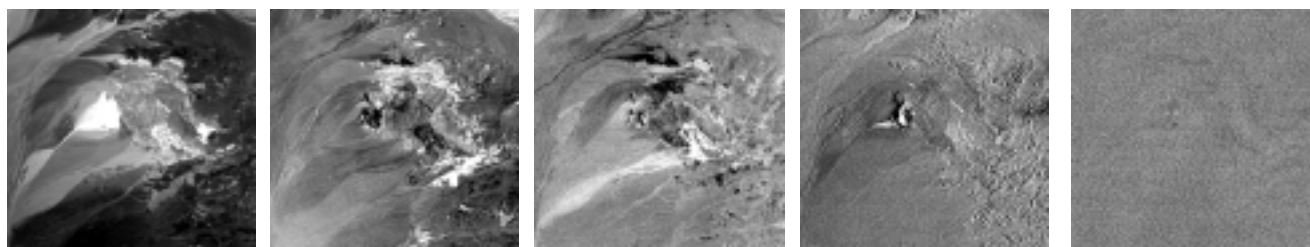


Figure 37: MNF images for the northern Death Valley AVIRIS SWIR data. Images from left to right, MNF band 1, MNF band 5, MNF band 8, MNF band 10, MNF band 20.



Figure 3: MNF images for the northern Death Valley Hyperion SWIR data. Images from left to right, MNF band 1, MNF band 5, MNF band 8, MNF band 10, MNF band 20.

The top MNF bands for each data set (20 for AVIRIS, 6 for Hyperion), which contain most of the spectral information (Green et al., 1988), were used to determine the most likely endmembers using the PPI procedure. These potential endmember spectra were loaded into an n-dimensional scatterplot and rotated in real time on the computer screen until “points” or extremities on the scatterplot were exposed (Boardman, 1993). These projections were “painted” using region-of-interest (ROI) definition procedures and then rotated again in 3 or more dimensions (3 or more MNF bands) to determine if their signatures were unique in the MNF data. Once a set of unique pixels were defined, then each separate projection on the scatterplot (corresponding to a pure endmember) was exported to a ROI in the image. Mean spectra were then extracted for each ROI from the apparent reflectance data to act as endmembers for spectral mapping (Figure 39). These endmembers were used for subsequent classification and other processing. Mixture-Tuned-Matched Filtering (MTMF), a spectral matching method (Boardman, 1998), was used to produce image-maps showing the distribution and abundance of selected minerals. (Note: MNF endmember spectra, not

reflectance spectra are used in the MTMF). The results are generally presented as gray-scale images (not shown) with values from 0 to 1.0, which provide a means of estimating mineral abundance. Brighter pixels in the images represent higher mineral abundances. Results images for both AVIRIS and Hyperion were produced by correcting the Hyperion data to match the AVIRIS spatial scale and orientation as described above. Selected results were combined as color-coded images to show the distribution of the principal (spectrally predominant) minerals (Figures 40 and 41). Minerals identified using the Hyperion data by comparison to a spectral library and previously verified by X-Ray Diffraction include calcite, dolomite, muscovite (3 varieties), silica, and zeolite (Kruse, 1988, 2003).

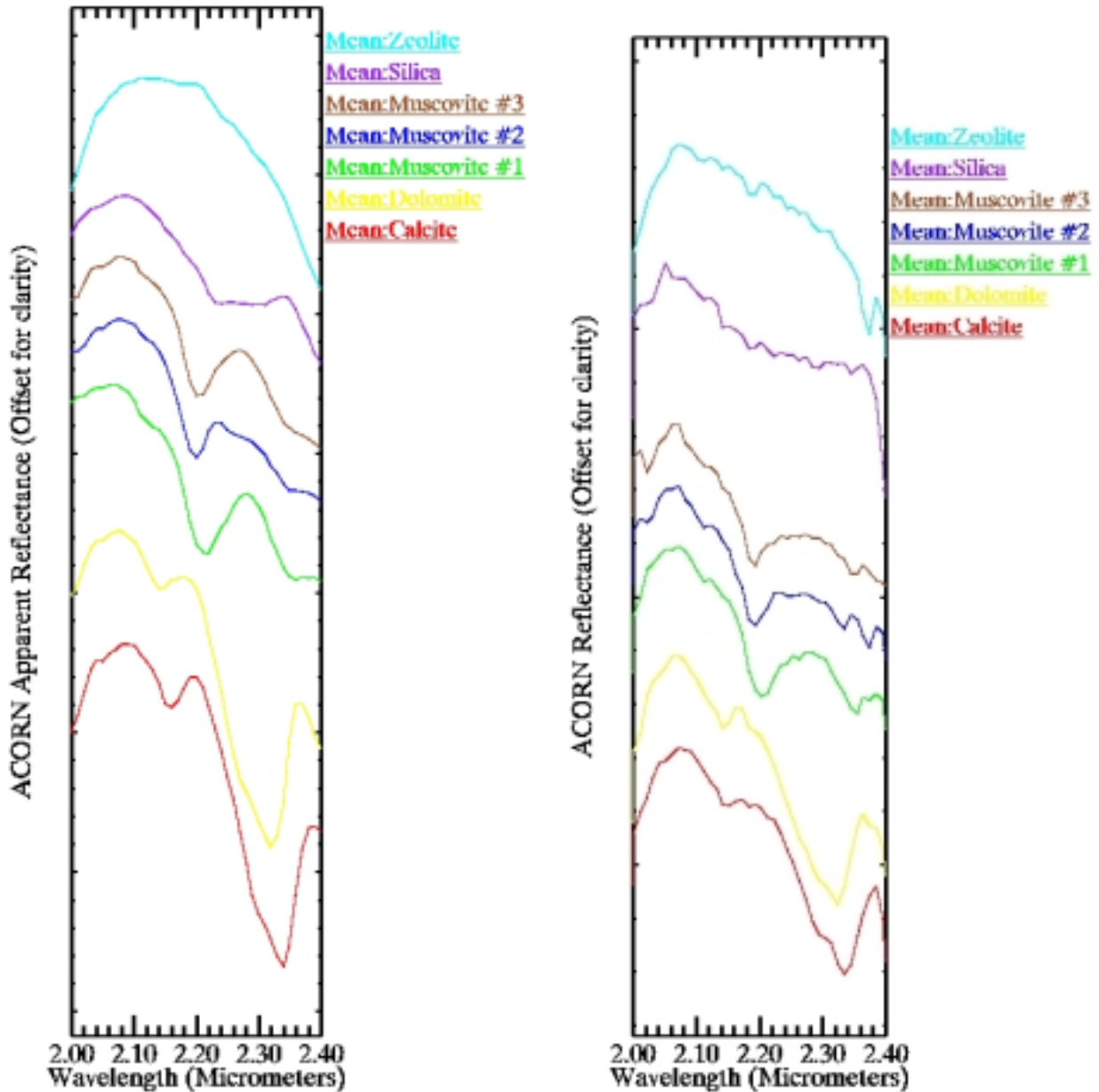


Figure 39: Endmember spectra extracted from the AVIRIS data (left) and Hyperion data (right).

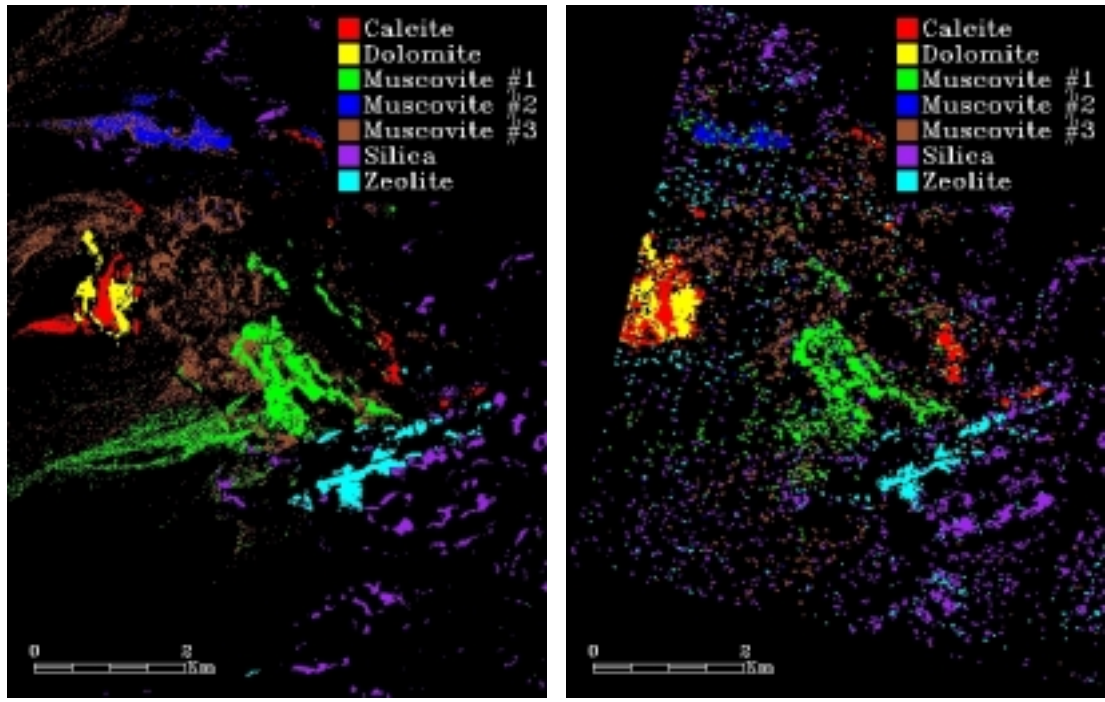


Figure 40: MTMF mineral maps for AVIRIS (left) and Hyperion (right) produced for the endmembers in Figure 4 for the northern Death Valley, California and Nevada site. Colored pixels show the spectrally predominant mineral at concentrations greater than 10%.

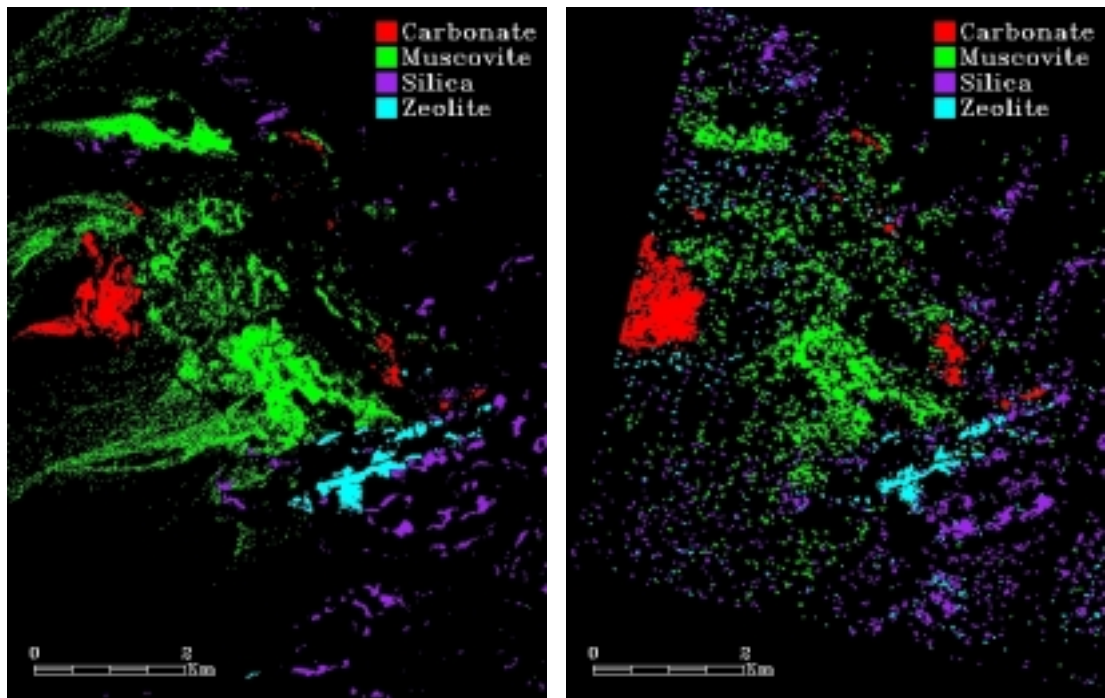


Figure 41: MTMF mineral maps for AVIRIS (left) and Hyperion (right) produced for a subset (combined) of the endmembers in Figure 4 for the northern Death Valley, California and Nevada site. Colored pixels show the spectrally predominant mineral group at concentrations greater than 10%.

Northern Death Valley Accuracy Assessment

Visual comparison of the detailed mapping results for the northern Death Valley site shows that Hyperion identifies similar minerals to AVIRIS and that there is generally good correspondence between the AVIRIS and Hyperion mapping. It is also possible to extract abundance information from both the AVIRIS and Hyperion data (Boardman and Kruse, 1994; Boardman et al., 1995, Kruse et al, 1999), but this is not illustrated here. Confusion matrix results comparing the AVIRIS and Hyperion mapping results, excluding the unclassified pixels show overall accuracy of approximately 76% for the Hyperion mapping as compared to AVIRIS, with a Kappa Coefficient of 0.71. Table 4 indicates that there is, however, considerable difficulty separating similar mineralogy. In this case, detecting and mapping the three muscovite varieties appears to be near the detection limit at the calculated 60:1 SNR of the Hyperion data. Grouping similar minerals together (calcite with dolomite, and combining the three muscovites) results in dramatic identification and mapping improvements (Figure 41, Table 5).

Table 4: Confusion Matrix comparing Hyperion northern Death Valley MTMF mineral mapping results to AVIRIS “Ground Truth” MTMF detailed mineral mapping results. Excludes unclassified pixels. Overall Accuracy is 76%. Kappa coefficient is 0.71

	AVIRIS Ground Truth (Percent)							
Hyperion Class	Calcite	Dolomite	Muscovite #1	Muscovite #2	Muscovite #3	Silica	Zeolite	Total
Calcite	82.66	16.75	0.00	0.31	1.11	0.46	0.21	11.46
Dolomite	15.73	83.01	0.00	0.00	0.00	0.09	0.10	9.74
Muscovite	0.10	0.00	85.62	15.04	41.13	1.37	0.00	33.07
Muscovite	0.00	0.00	2.11	76.43	11.49	0.09	0.00	8.62
Muscovite	0.10	0.00	8.33	4.50	35.65	2.46	0.72	10.14
Silica	0.20	0.24	3.81	3.72	6.36	89.70	6.00	14.76
Zeolite	1.21	0.00	0.13	0.00	4.26	5.83	92.96	12.21
Total	100.00	100.00	100.00	100.00	100.00	100.00	100.00	100.00

Table 5: Confusion Matrix comparing Hyperion northern Death Valley MTMF mapping results to AVIRIS “Ground Truth” MTMF basic (Combined Minerals) mapping results. Excludes unclassified pixels. Overall Accuracy is 94%. Kappa coefficient is 0.91.

Hyperion Class	AVIRIS Ground Truth (Percent)				
	Carbonate	Muscovite	Silica	Zeolite	Total
Carbonate	99.01	0.44	0.55	0.31	21.19
Muscovite	0.11	93.23	3.92	0.72	51.83
Silica	0.22	4.72	89.70	6.00	14.76
Zeolite	0.66	1.61	5.83	92.96	12.21
Total	100.00	100.00	100.00	100.00	100.00

Confusion Matrix comparisons between AVIRIS and Hyperion show:

- Slight problem mapping unclassified pixels on AVIRIS as minerals on Hyperion (~1-5%)
- Larger problem missing pixels shown as specific mineralogy on AVIRIS and mapping them as unclassified on Hyperion (30 - 90% depending on mineral) (fine distinctions such as 3 muscovites have high errors illustrating that SNR makes ID and mapping problematic for some minerals)
- When all NDV endmembers are considered and only the classified pixels are compared, Hyperion matches AVIRIS to approximately the 80 - 90% level with lower matches for problem minerals
- Grouping Hyperion classified minerals into more general groups (eg: muscovite, carbonate) results in significant improvement with Hyperion match to AVIRIS at approximately >90% level. Carbonates match at +99%.
- Hyperion SWIR SNR at the NGM, NV, site of approximately 60:1 allows improved mineral identification and within-species variability mapping compared to Hyperion data sets with lower SNR

The figures and tables above demonstrate Hyperion’s utility for mapping specific earth-surface materials (minerals) using AIG’s standardized hyperspectral analysis methods. In this case, the data allow separation and identification of several very similar spectral signatures based on absorption features near 2.2 – 2.3 μm . Comparison to airborne hyperspectral data indicates that Hyperion performs with approximately 80-95% accuracy with respect to mineral maps produced using the same approach and verified utilizing field mapping and ground-based spectral measurements (Kruse et al., 2002a, 2003).

4.0 SUMMARY OF KEY RESEARCH RESULTS

The following presents the key results from the main EO-1 Hyperion geologic study sites used for this analysis/research.

- Los Menucos Argentina: represents a case where Hyperion data collected during the winter season (low solar zenith angle) lack sufficient SNR (<40:1 VNIR, <15:1 SWIR) for accurate mineral mapping.
- Cuprite, NV: an “Early” Hyperion acquisition for the northern hemisphere (a winter scene). SWIR SNR is approximately 25:1. Hyperion analysis and comparison to known geology derived from AVIRIS data and ancillary ground measurements validate Hyperion basic mineral mapping. Some confusion occurs between similar minerals.
- Virginia City, NV: General mineral mapping using Hyperion possible, however, some minerals missed, and similar minerals confused. SWIR SNR is particularly low (approximately 20:1) principally because of lower albedo, vegetated, heterogeneous, mountainous, mixed terrain. Limited separation of cation-substituted micas is possible. Particular problems mapping 2.3 μm minerals such as chlorite, epidote, amphiboles, carbonates.
- Oatman, AZ: Hyperion successfully maps basic mineral groups (kaolinite, alunite, chlorite and muscovites) and detects and maps subspecies (cation substitution) of muscovites. Hyperion was unable to fully separate calcite from chlorite and did not detect dolomite or dickite (probable SNR issues).
- N. Grapevine Mtns, NV (northern Death Valley site) is a “best case” Hyperion acquisition from the N. Hemisphere Summer (July 2001). SWIR SNR is approximately 60:1. The higher SNR allows improved mineral identification and within-species variability mapping compared to Hyperion data sets with lower SNR.

Other key results of this research include:

- Validation of methods developed for analysis of airborne hyperspectral data for analysis of spaceborne HSI data (“hands-off” analysis using model-based atmospheric correction and n-Dimensional scatterplot approach)
- Demonstration and validation of HSI mineral mapping from space for a variety of geologic environments
 - Basic Mineral Mapping performed for minerals with high spectral contrast @ >90% Accuracy for pixels mapped as specific mineral
 - Basic Mineral Mapping for similar minerals (eg: MgOH vs Carbonate minerals) but some problems at lower SNR
 - Within-Species variability (cation-substitution), but lower accuracy dependent on spectral feature similarity and SNR
 - Establishment of effective Hyperion SWIR SNR as ~60:1 for mid-latitude, summer Hyperion scenes and as low as ~15:1 for similar winter scenes. Results illustrate requirement for higher SNR for future spaceborne systems

5.0 RESEARCH SIGNIFICANCE

The AIG/CSIRO proposal was for evaluation, validation, and demonstration of Hyperion's capabilities for geologic mapping and mineral resource assessment, offering a low-cost, high-experience, high-leverage approach. The effort drew heavily on previous work and outside funding sources to maximize the cost-effectiveness for the Hyperion evaluation and validation. Examining Hyperion data collected over well-understood geological sites resulted in practical and important demonstrations of Hyperion data for geological mapping and mineral resource assessment. Validation of the spatial, spectral and radiometric performance of Hyperion was achieved using real-world applications as the defining metric. Additionally, analysis methods originally developed for airborne hyperspectral data were validated for use with satellite-based sensors. The following points illustrate the significance of this research:

- These Hyperion geologic case histories demonstrate the analysis methodologies and level of information available from Hyperion for mineral mapping
- AIG's/CSIRO's hyperspectral data processing methods applied to Hyperion data lead to definition of specific key minerals and mineral assemblages
- Hyperion analysis and comparison to known geology derived from AVIRIS data and ancillary ground measurements generally validate on-orbit mineral mapping and Hyperion performance
- Hyperion's lower SWIR SNR compared to AVIRIS results in lower data dimensionality, thus fewer endmembers can be identified and mapped than with AVIRIS
- Relatively low Hyperion SWIR SNR limits effectiveness for many datasets, placing them at the margin of operational utility (Some minerals mapped, others missed)
- Hyperion often confuses similar minerals that are separable using AVIRIS
- "Success" evident in "summer" (high-solar zenith angle) data for near-100% exposed, high-albedo areas with little mixing and little vegetation
- Results from AIG/CSIRO's primary test sites demonstrate that more detailed within-species mineral identification and mapping is possible in some cases under optimum acquisition conditions
- Even with the SNR problems noted, Hyperion is a success as a technology demonstration. It performs well under most circumstances for basic mineral identification/mapping
- Hyperion has acted as a valuable learning experience for the future of spaceborne hyperspectral imaging. Our (and others) Hyperion analyses illustrate that improved performance (principally SNR) is required for typical geologic applications. Future satellite systems will need to be enhanced to improve overall mapping performance, the capability to make detailed mineralogical distinctions, and "all-season" mapping capabilities

6.0 KRUSE ET AL., EO-1 HYPERION PUBLICATIONS

- Kruse, F. A., 2003, District-level mineral survey using airborne hyperspectral data, Los Menucos, Argentina: *Annals of Geophysics* (Abstract accepted, full paper to be submitted by 04/12/2003).
- Kruse, F. A., Boardman, J. W., Huntington, J. F., Mason, P., and Quigley, M.A., 2003, Evaluation and Validation of EO-1 Hyperion for Geologic Mapping: in Special Issue, *TGARSS, IEEE* (Submitted 6/2002, Revised 11/2002, Accepted for Publication 01/27/2003)
- Kruse, F. A., 2003, Hyperspectral mapping of coral reef systems using EO-1 Hyperion, Buck Island, U. S. Virgin Islands: *Coral Reefs, Special Issue on Remote Sensing of Coral Reefs* (Submitted 03/7/2003).
- Kruse, F. A., 2003, Mineral Mapping with AVIRIS and EO-1 Hyperion: In proceedings 12th JPL Airborne Geoscience Workshop, Jet Propulsion Laboratory, 24 –28 February 2003, Pasadena, CA (in press)
- Kruse, F. A., 2003, Preliminary Results – Hyperspectral mapping of coral reef systems using EO-1 Hyperion, Buck Island, U.S. Virgin Islands: In proceedings 12th JPL Airborne Geoscience Workshop, Jet Propulsion Laboratory, 24 –28 February 2003, Pasadena, CA (in press)
- Kruse, F. A., Boardman, J. W., Huntington, J. F., Mason, P., and Quigley, M.A., 2002, Evaluation and Validation of EO-1 Hyperion for Geologic Mapping: in Proceedings, *IGARSS 2002*, 24 – 28 June 2002, Toronto, Canada , Published on CD ROM – Paper 02_06_17:00, ISBN: 0-7803-7537-8. Also in hardcopy, v. I, p. 593-595, IEEE Operations Center, Piscataway, NJ.
- Kruse, F. A., Comparison of AVIRIS and Hyperion for Hyperspectral Mineral Mapping, 2002, In proceedings 11th JPL Airborne Geoscience Workshop, Jet Propulsion Laboratory, 4-8 March 2002 (in press).
- Kruse F. A., Perry, S. L., and Caballero, A., 2002, Integrated Multispectral and Hyperspectral Mineral Mapping, Los Menucos, Rio Negro, Argentina, Part I: Landsat TM Reconnaissance and AVIRIS Prospect Mapping: In proceedings 11th JPL Airborne Geoscience Workshop, Jet Propulsion Laboratory, 4-8 March 2002 (in press).
- Kruse F. A., Perry, S. L., and Caballero, A., 2002, Integrated Multispectral and Hyperspectral Mineral Mapping, Los Menucos, Rio Negro, Argentina, Part II: EO-1 Hyperion/AVIRIS Comparisons and Landsat TM/ASTER Extensions: In proceedings 11th JPL Airborne Geoscience Workshop, Jet Propulsion Laboratory, 4-8 March 2002 (in press).
- Kruse, F. A., Boardman, J. W., and Huntington, J. F., 2002, Comparison of Airborne and Satellite Hyperspectral Data for Geologic Mapping: in Proceedings, *SPIE International Symposium on AeroSense*, 1-5 April 2002, Orlando, FL, v. 4725, p. 128-139.
- Kruse, F. A., Boardman, J. W., and Huntington, J. F., 2002, Comparison of EO-1 Hyperion and Airborne Hyperspectral Remote Sensing Data for Geologic Applications: in Proceedings, *IEEE Aerospace Conference*, 9-16 March 2002, Big Sky, Montana , published on CD-ROM, IEEE Catalog Number 02TH8593C, Paper #6.0102, 12 p.

Kruse, F. A., Boardman, J. W., and Huntington, J. F., 2001, Progress Report: Geologic Validation of EO-1 Hyperion: in Proceedings of the 10th JPL Airborne Earth Science Workshop: Jet Propulsion Laboratory Publication 02-1, p. 253 – 265.

7.0 ACKNOWLEDGMENTS

This research was only partially funded by NASA under grant NCC5-495. Additional financial support was provided in the form of matching internal research and development funds (IR&D) funds by Analytical Imaging and Geophysics LLC. CSIRO Exploration and Mining's participation in the project was at no cost to NASA – funded by CSIRO. AVIRIS data for various test sites were acquired by JPL for previous NASA-funded studies. Additional AVIRIS data were acquired under this grant for the Los Menucos, Argentina Site. HyMap data used for this study are courtesy of AIG and HyVista Corporation. Amer Smailbegovic (University of Nevada Reno) assisted with field spectral measurements at Steamboat Springs, Nevada. Sandra Perry (Perry Remote Sensing) suggested the Argentina validation site and participated in analysis and field verification at no cost to NASA. Rio Tinto Mining (RTZ) provided partial funding, vehicles, lodging, and field support in Argentina. JPL provided an ASD field spectrometer for spectral measurements in Argentina. ACORN is a trademark of ImSpec Associates, LLC. ENVI is a registered trademark of Research Systems Inc., Boulder, Colorado. Pixel Purity Index (PPI), n-Dimensional Visualizer, Spectral Analyst, and Mixture-Tuned Matched Filter (MTMF) are all trademarks of Research Systems Inc.

8.0 REFERENCES CITED

- Abrams, M. J., R. P. Ashley, L. C. Rowan, A. F. H. Goetz, and A. B. Kahle, 1978. Mapping of hydrothermal alteration in the Cuprite Mining District, Nevada using aircraft scanner images for the spectral region 0.46 - 2.36 μm , Geology, 5., 173 - 178.
- Albers, J. P., and Stewart, J. H., 1972, Geology and mineral deposits of Esmeralda County, Nevada: Nevada Bureau of Mines and Geology Bulletin 78, 80 p.
- Analytical Imaging and Geophysics LLC (AIG), 2001, ACORN User's Guide, Stand Alone Version: Analytical Imaging and Geophysics LLC, 64 p.
- Ashley, R. P., and Abrams, M. J., 1980, Alteration mapping using multispectral images-Cuprite Mining District, Esmeralda County, Nevada: U. S. Geological Survey Open File Report 80-367, 17 p.
- Boardman, J. W., 1989. Inversion of imaging spectrometry data using singular value decomposition: in Proceedings IGARSS '89, 12th Canadian Symposium on Remote Sensing, Vol. 4, pp. 2069 - 2072.
- Boardman, J. W., 1993, Automated spectral unmixing of AVIRIS data using convex geometry concepts: in Summaries, Fourth JPL Airborne Geoscience Workshop, JPL Publication 93-26, v. 1, p. 11 - 14.
- Boardman, Joseph, 1998, Leveraging the high dimensionality of AVIRIS data for improved sub-pixel target unmixing and rejection of false positives: mixture tuned matched filtering, in: Summaries of the Seventh Annual JPL Airborne Geoscience Workshop, Pasadena, CA, JPL Publication 97-21, v. 1, p. 55.

- Boardman, J. W., and Kruse, F. A., 1994, Automated spectral analysis: A geological example using AVIRIS data, northern Grapevine Mountains, Nevada: in Proceedings, Tenth Thematic Conference, Geologic Remote Sensing, 9-12 May 1994, San Antonio, Texas, p. I-407 - I-418.
- Boardman, J. W., Kruse, F. A., and Green, R. O., 1995, Mapping target signatures via partial unmixing of AVIRIS data: in Summaries, Fifth JPL Airborne Earth Science Workshop, JPL Publication 95-1, v. 1, p. 23-26.
- Boardman, J. W., and Huntington, J.F., 1996, Mineral mapping with 1995 AVIRIS data, in: Summaries of the Sixth Annual JPL Airborne Geoscience Workshop, Pasadena, CA, JPL Publication 96-4. v. 1, p. 9 – 11.
- Center for the Study of Earth from Space (CSES), 1999, Atmosphere REMoval Program (ATREM) User's Guide, Version 3.1, Center for the Study of Earth from Space, Boulder, Colorado, 31 p.
- Clark, R. N., T. V. V. King, M. Klejwa, and G. A. Swayze, 1990. High spectral resolution spectroscopy of minerals: J. Geophys. Res., 95 (B8), 12653 - 12680.
- Clark, R.N., Swayze, G.A., Gallagher, A., King, T.V.V., and Calvin, W.M., 1993, The U. S. Geological Survey Digital Spectral Library: Version 1: 0.2 to 3.0 μm : U. S. Geological Survey, Open File Report 93-592, 1340 p.
- Clifton, C.G., Buchanan, L.J. and Durning, W.P., 1980 Exploration Procedure and Controls of Mineralisation in the Oatman Mining District, Oatman, Arizona: New York, So. Of Mining Engineers of AIME, Reprint, 80-143, 17 pages.
- Collwell, R. N. (ed.), 1983, Manual of Remote Sensing, 2nd Edition, American Society of Photogrammetry and Remote Sensing (ASPRS), pp. 344-363, and pp. 1196.
- Chrien, T. G., Green, R. O., Boardman, J. W., Chippendale, B., Chovit, C. J., Eastwood, M., Faust, J. A., Finn, M., Hall, P., Holbrook, J., Houston, J., Kurzweil, c., Longenecker, J., Raney, J., Sarture, C., and Tuell, G. (1999) Operation of NASA's Airborne Visible/Infrared Imaging Spectrometer (AVIRIS) on a NOAA Twin Otter: Program Review: in Proceedings of the 8th JPL Airborne Earth Science Workshop: Jet Propulsion Laboratory Publication.
- Franco, S., Puente, N., Varela, C., Gemuts, I., 2000, Mineralizacion Aurifera en El Distrito Los Menucos, Provincia de Rio Negro, Argentina: in Proceedings, Argentina Mining 2000, Mendoza, Argentina, August 22 - 25, 2000, p. 112 - 126.
- Gao B. and Goetz, A. F. H. (1990). "Column atmospheric water vapor and vegetation liquid water retrievals from airborne imaging spectrometer data. Journal of Geophysical Research, 95(D-4): p. 3549-3564.
- Gemuts, I., and Perry, S., 2000, Los Menucos Au District, Rio Negro Province, Argentina: Abstract and Presentation, Northwest Mining Association, Spokane, Washington, December 7 - 10, 2000.
- Goetz, A. F. H., and B. Kindel, 1996. Understanding unmixed AVIRIS images in Cuprite, NV using coincident HYDICE data, in Summaries of the 6th Annual JPL Airborne Earth Science

- Workshop, JPL Pub. 96-4, Vol. 1. AVIRIS Workshop, Jet Propulsion Laboratory, California Institute of Technology, Pasadena, Calif., pp. 97-103.
- Goetz, A. F. H., Vane, G., Solomon, J. E., and Rock, B. N., 1985, Imaging spectrometry for earth remote sensing: Science, 228, 1147-1153.
- Goetz, A. F. H., and Strivastava, V., 1985, Mineralogical mapping in the Cuprite mining district: in Proceedings of the Airborne Imaging Spectrometer (AIS) Data Analysis Workshop, JPL Publication 85-41, p. 22-29.
- Green, A. A., Berman, M., Switzer, B., and Craig, M. D., 1988, A transformation for ordering multispectral data in terms of image quality with implications for noise removal: IEEE Transactions on Geoscience and Remote Sensing, v. 26, no. 1, p. 65 - 74.
- Green, R. O., B. Pavri, J. Faust, and O. Williams, 1999, "AVIRIS radiometric laboratory calibration, inflight validation, and a focused sensitivity analysis in 1998," in Proceedings of the 8th JPL Airborne Earth Science Workshop: Jet Propulsion Laboratory Publication 99-17, p. 161 – 175.
- Green, R. O., Chrien, T. G., and Pavri, B., 2003, "On-orbit Determination of the Radiometric and Spectral Calibration of Hyperion Using Ground, Atmospheric and AVIRIS Underflight Measurements," TGARS Special Issue on EO-1 (in press).
- Harsanyi, J. C., and Chang, C. I., 1994, Hyperspectral image classification and dimensionality reduction: An orthogonal subspace projection approach: IEEE Trans. Geosci. and Remote Sens., v. 32, p. 779-785.
- Henkle, W. R., John, T. W., and Hyde, C. C., 1993. Geochemical and geophysical signatures at three precious metals exploration targets in Nevada. Journal of Geochemical Exploration 47, 29-43.
- Hook, S. J., 1990; The combined use of multispectral remotely sensed data from the short wave infrared (SWIR) and thermal infrared (TIR) for lithological mapping and mineral exploration: in Proceedings, Fifth Australasian Remote Sensing Conference, Perth, Western Australia, v. 1, p. 371 – 380.
- Kruse, F. A., 1988, Use of Airborne Imaging Spectrometer data to map minerals associated with hydrothermally altered rocks in the northern Grapevine Mountains, Nevada and California: Remote Sensing of Environment, v. 24, no. 1, pp. 31-51.
- Kruse, F. A., Kierein-Young, K. S., and Boardman, J. W., 1990, Mineral mapping at Cuprite, Nevada with a 63 channel imaging spectrometer: Photogrammetric Engineering and Remote Sensing, v. 56, no. 1, p. 83-92.
- Kruse, F. A., Lefkoff, A. B., and Dietz, J. B., 1993a, Expert System-Based Mineral Mapping in northern Death Valley, California/Nevada using the Airborne Visible/Infrared Imaging Spectrometer (AVIRIS): Remote Sensing of Environment, Special issue on AVIRIS, May-June 1993, v. 44, p. 309 - 336.
- Kruse, F. A., Lefkoff, A. B., Boardman, J. B., Heidebrecht, K. B., Shapiro, A. T., Barloon, P. J., and Goetz, A. F. H., 1993b, The Spectral Image Processing System (SIPS) - Interactive

Visualization and Analysis of Imaging Spectrometer Data: Remote Sensing of Environment, Special issue on AVIRIS, May-June 1993, v. 44, p. 145 - 163.

- Kruse, F. A., Huntington, J. H., and Green, R. O., 1996a, Results from the 1995 AVIRIS Geology Group Shoot: in Proceedings, 2nd International Airborne Remote Sensing Conference and Exhibition: Environmental Research Institute of Michigan (ERIM), Ann Arbor, v. I, p. I-211 - I-220.
- Kruse, F. A., Boardman, J. W., and Huntington, J. H., 1996b, The 1995 Geology AVIRIS Group Shoot: in Proceedings, 6th JPL Airborne Earth Science Workshop: Jet Propulsion Laboratory Publication 96-4, v. 1, p. 155 - 166.
- Kruse, F. A., 1997, Regional Geologic Mapping Along the Colorado Front Range from Ft Collins to Denver Using the Airborne Visible/Infrared Imaging Spectrometer (AVIRIS): in Proceedings, 12th Thematic Conference, Applied Geologic Remote Sensing, 17-19 November 1997, Environmental Research Institute of Michigan (ERIM), Ann Arbor, MI, p. II-91 – II-98.
- Kruse, F. A., Boardman, J. W., and Huntington, J. F., 1999, Fifteen Years of Hyperspectral Data: northern Grapevine Mountains, Nevada: in Proceedings of the 8th JPL Airborne Earth Science Workshop: Jet Propulsion Laboratory Publication (in press).
- Kruse, F. A., Boardman, J. W., Lefkoff, A. B., Young, J. M., Kierein-Young, K. S., Cocks, T. D., Jenssen, R., and Cocks, P. A., 2000, HyMap: An Australian Hyperspectral Sensor Solving Global Problems – Results from USA HyMap Data Acquisitions: in Proceedings of the 10th Australasian Remote Sensing and Photogrammetry Conference, Adelaide, Australia, 21-25 August 2000, Causal Productions (www.causalproductions.com), published on CD-ROM.
- Kruse, F. A., Boardman, J. W., and Huntington, J. F., 2001, Progress Report: Geologic Validation of EO-1 Hyperion: in Proceedings of the 10th JPL Airborne Earth Science Workshop: Jet Propulsion Laboratory Publication 02-1, p. 253 – 265.
- Kruse, F. A., Boardman, J. W., and Huntington, J. F., 2002a, Comparison of EO-1 Hyperion and Airborne Hyperspectral Remote Sensing Data for Geologic Applications: in Proceedings, IEEE Aerospace Conference, 9-16 March 2002, Big Sky, Montana, published on CD-ROM, IEEE Catalog Number 02TH8593C, Paper #6.0102, 12 p.
- Kruse F. A., Perry, S. L., and Caballero, A., 2002b, Integrated Multispectral and Hyperspectral Mineral Mapping, Los Menucos, Rio Negro, Argentina, Part I: Landsat TM Reconnaissance and AVIRIS Prospect Mapping: In proceedings 11th JPL Airborne Geoscience Workshop, 4-8 March 2002, Pasadena, CA, Jet Propulsion Laboratory Publication 03-4 (CD-ROM).
- Kruse F. A., Perry, S. L., and Caballero, A., 2002c, Integrated Multispectral and Hyperspectral Mineral Mapping, Los Menucos, Rio Negro, Argentina, Part II: EO-1 Hyperion/AVIRIS Comparisons and Landsat TM/ASTER Extensions: In proceedings 11th JPL Airborne Geoscience Workshop, 4-8 March 2002, Pasadena, CA, Jet Propulsion Laboratory Publication 03-4 (CD-ROM).
- Kruse, F. A., Boardman, J. W., Huntington, J. F., Mason, P., and Quigley, M.A., 2002d, Evaluation and Validation of EO-1 Hyperion for Geologic Mapping: in Proceedings, IGARSS 2002, 24

– 28 June 2002, Toronto, Canada , Published on CD ROM – Paper 02_06_17:00, ISBN: 0-7803-7537-8. Also in hardcopy, v. I, p. 593-595, IEEE Operations Center, Piscataway, NJ.

- Kruse, F. A., 2002, Comparison of AVIRIS and Hyperion for Hyperspectral Mineral Mapping: In proceedings 11th JPL Airborne Geoscience Workshop, 4-8 March 2002, Pasadena, CA, Jet Propulsion Laboratory Publication 03-4 (CD-ROM).
- Kruse, F. A., 2003, Mineral Mapping with AVIRIS and EO-1 Hyperion: In proceedings 12th JPL Airborne Geoscience Workshop, Jet Propulsion Laboratory, 24 –28 February 2003, Pasadena, CA (in press)
- Kruse, F. A., Boardman, J. W., Huntington, J. F., Mason, P., and Quigley, M.A., 2003, Evaluation and Validation of EO-1 Hyperion for Geologic Mapping: in Special Issue, TGARSS, IEEE (in press)
- Moring, B., 1986, Reconnaissance surficial geologic map of northern Death Valley, California and Nevada: U. S. Geological Survey Miscellaneous Field Studies Map MF-1770, 1:62,500, 1 sheet.
- Pearlman, J, Stephen Carman, Paul Lee, Lushalan Liao and Carol Segal, 1999, Hyperion Imaging Spectrometer on the New Millennium Program Earth Orbiter-1 System: In Proceedings, International Symposium on Spectral Sensing Research (ISSSR), Systems and Sensors for the New Millennium, published on CD-ROM, International Society for Photogrammetry and Remote Sensing (ISPRS).
- Perry, S., and Gemuts, I., 2000, New High Sulfidation Gold District: Los Menucos, rio Negro Province, Argentina - A Landsat Discovery: Presented at Fourteenth International Conference, Applied Geologic Remote Sensing, November 6 - 8, 2000, Las Vegas, Nevada, Veridian ERIM International.
- Research Systems Inc (RSI), 2001, ENVI User's Guide, Research Systems Inc, 948 p.
- Richards, J.A., 1994, Remote Sensing Digital Image Analysis, An Introduction, Springer-Verlag, New York, pp. 271 – 275.
- Schoen, R., and White, D. E., (1967). "Hydrothermal alteration of basaltic andesite and other rocks in drill hole GS-6, Steamboat Springs, Nevada. U.S. Geological Survey Professional Paper 575-B: p. 110-119.
- Schoen, R., White, D. E., and Hemley, J.J. (1974). "Argillization by descending acid at Steamboat Springs, Nevada." Clays and Clay Minerals 22: p. 1-22.
- Sigvaldason, G. E., and White, D. E. (1962). "Hydrothermal alteration in drill holes GS-5 and GS-7, Steamboat Springs, Nevada." U.S. Geological Survey Professional Paper 450-D: D113-D117.
- Silberman, M. L., White, D. E., Keith, T. E. C., and docktor, R. D. (1979). Duration of hydrothermal activity at Steamboat Springs, Nevada , from ages of the spacially associated volcanic rock. U. S. Geological Suvey Professional Paper 458-D: 14 p.

- Shipman, H. and Adams, J. B., 1987, Detectability of minerals on desert alluvial fans using reflectance spectra, Journal of Geophysical Research, v. 92, no. B10, p. 10391-10402.
- Swayze, G. A., Clark, R. L., Sutley, S. and Gallagher, A. J., 1992, Ground-truthing AVIRIS mineral mapping at Cuprite, Nevada: in Summaries of the Third Annual JPL Airborne Geosciences Workshop, V 1., AVIRIS Workshop, JPL Publication 92-14, p. 47 – 49.
- Swayze, G. A., 1997. The hydrothermal and structural history of the Cuprite Mining District, Southwestern Nevada: An integrated geological and geophysical approach: Unpublished Ph. D. thesis, University of Colorado, Boulder, Co, 341 pp.
- Thorson, J.P., 1971, Igneous Petrology of the Oatman Mining District, Mohave County, Arizona, Unpublished Ph.D dissertation, Uni. California, Santa Barbara, 189 pages.
- Thompson, J.V., 1956, Geology of the Virginia City Quadrangle, Nevada, USGS Bull. 1042-C, 75 pages.
- Vikre, P.G. 1989. Fluid-mineral relations in the Comstock Lode. Economic Geology 84, 1574-1613.
- Vikre, P.G. 1998. Quartz-alunite alteration in the western part of the Virginia Range, Washoe and Storey Counties, Nevada. Economic Geology 93, 338-346.
- Vikre P.G. McKee E.H. & Silberman M.L. 1988. Chronology of Miocene hydrothermal and igneous events in the western Virginia Range, Washoe, Storey, and Lyon counties, Nevada. Economic Geology 83, 864-874.
- Whitebread, D.H. 1976. Alteration and Geochemistry of Tertiary Volcanic Rocks in Parts of the Virginia City Quadrangle, Nevada. US Geological Survey Professional Paper No 936.
- White, D. E. (1955). “Thermal springs and epithermal ore deposits.” Economic Geology Fiftieth Anniversary Volume: p. 99-154.
- White, D. E., Anderson, E. T., and Grubbs, D. K.. (1963). “Geothermal brine well/mile-deep drill hole may tap ore-bearing magmatic water and rocks undergoing metamorphism.” Science 139(p. 919-922).
- White, D. E., Thompson, G. A., and Sanberg, C. S. (1964). “Rocks, structure, and geologic history of Steamboat Springs thermal area, Washoe County, Nevada.” U. S. Geological Survey Professional Paper 458-B: 63 p.
- White, D. E. (1967). “Some principles of geyser activity, mainly from Steamboat Springs, Nevada.” American Journal of Science 265(8): p. 641-684.
- White, D. E. (1968). “Hydrology, activity, and heat flow of the Steamboat Springs thermal systems, Washoe County, Nevada.” U. S. Geological Survey Professional Paper 458-C: 109 p.
- White, D. E. (1981). “Active Geothermal Systems and Hydrothermal Ore Deposits.” Economic Geology 75th Anniversary Volume: p. 392-423.

- White, d. E., Hutchinson, R. A., and Keith, T.E.C. (1988). "The geology and remarkable thermal activity of Norris Geyser Basin, Yellowstone National Park, Wyoming." U.S. Geological Survey Professional Paper 1456: 84 p.
- White, D. E., Heropoulos, C., and Fournier, R. O. (1992). "Gold and other minor elements associated with the hot springs and geysers of Yellowstone National Park, Wyoming, supplemented with data from Steamboat Springs, Nevada." U.S. Geological Survey Bulletin 2001: 19 p.
- Wrucke, C. T., Werschkey, R. S., Raines, G. L., Blakely, R. J., Hoover, D. B., and Miller, M. S., 1984, "Mineral resources and mineral resource potential of the Little Sand Spring Wilderness Study Area, Inyo County, California," U. S. Geological Survey Open File Report 84-557, 20 p.